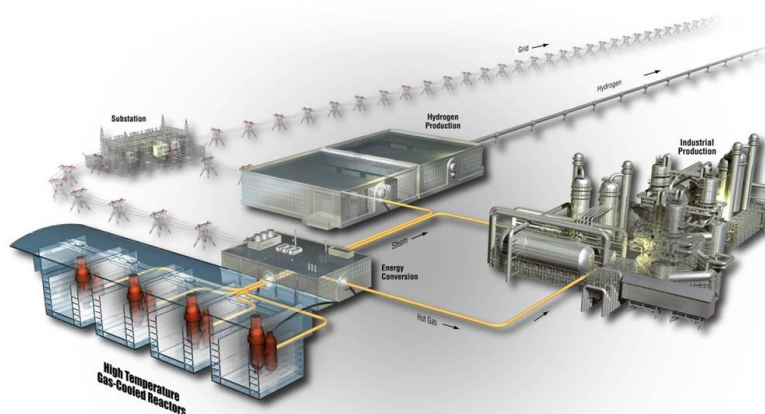




Electron Microscopic Examination of Irradiated AGR-2 TRISO-Coated Particle AGR2-222-RS019

Changing the World's Energy Future

Subhashish Meher
Isabella van Rooyen



DISCLAIMER

This information was prepared as an account of work sponsored by an agency of the U.S. Government. Neither the U.S. Government nor any agency thereof, nor any of their employees, makes any warranty, expressed or implied, or assumes any legal liability or responsibility for the accuracy, completeness, or usefulness, of any information, apparatus, product, or process disclosed, or represents that its use would not infringe privately owned rights. References herein to any specific commercial product, process, or service by trade name, trademark, manufacturer, or otherwise, does not necessarily constitute or imply its endorsement, recommendation, or favoring by the U.S. Government or any agency thereof. The views and opinions of authors expressed herein do not necessarily state or reflect those of the U.S. Government or any agency thereof.

**Electron Microscopic Examination of an Irradiated TRISO-Coated
Particle of AGR-2 Experiment: AGR2-222-RS019**

**Subhashish Meher
Isabella van Rooyen**

November 2020

**Idaho National Laboratory
Advanced Reactor Development
Idaho Falls, Idaho 83415**

<http://www.art.inl.gov>

**Prepared for the
U.S. Department of Energy
Office of Nuclear Energy
Under DOE Idaho Operations Office
Contract DE-AC07-05ID14517**

Page intentionally left blank

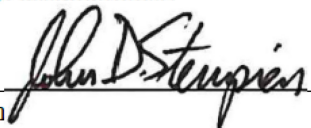
INL ARD Program

Electron Microscopic Examination of an Irradiated TRISO-Coated Particle of AGR-2 Experiment: AGR2-222-RS019

INL/EXT-20-60569
Revision 0

November 2020

Technical Reviewer: (Confirmation of mathematical accuracy, and correctness of data and appropriateness of assumptions.)



John D. Stempien
ARD AGR PIE Technical Lead

11/24/2020

Date

Approved by:



Paul A. Demkowicz
AGR Program Technical Director

11/25/2020

Date



Gerhard Strydom
ARD Co-National Technical Director

11/30/2020

Date



Michelle T. Sharp
INL Quality Assurance

11/25/2020

Date

ABSTRACT

This report presents the transmission electron microscopic (TEM) examination of an irradiated tristructural isotropic (TRISO) coated particle from Compact 2-2-2 from the second Advanced Gas Reactor experiment (AGR-2). The examination of particle AGR2-222-RS019 is focused on the interface between the silicon carbide (SiC) and inner pyrolytic carbon (IPyC) layer, the central part of SiC, and the interface between SiC and outer pyrolytic carbon (OPyC) layer. The SiC grain boundary distribution and associated fission product precipitates were characterized by scanning transmission electron microscopy (STEM), energy dispersive spectroscopy (EDS), and precession electron diffraction (PED) in the TEM. Two separate locations on the SiC layer, adjacent to intact and broken buffer layer, were selected in the irradiated TRISO particle. The key observation in this particle is that the compositional nature of grain boundary precipitates is more complex near IPyC/SiC layer where Pd, Pd-Ag, Pd-U containing precipitates can be observed. However, the compositions of precipitates towards the outermost region of SiC is mainly Pd. Ag has been observed in the IPyC/SiC layer in one of the two locations. The comparison of our results to previously irradiated and analyzed, Variant 3, safety-tested at 1600°C, AGR-1 TRISO particles (AGR1-433-001 and AGR1-433-004) showed that the grain boundary distributions have some noticeable differences. The differences in coincident site lattice grain boundary and misorientation angles are possibly inherent to the fabrication process. Neutron-irradiation-induced void distribution has been found to be non-uniform. A high concentration of smaller voids is found at the stacking faults compared to those in the bulk SiC. Larger void sizes are observed in the SiC location that is near to the broken buffer layer. This void size variation with the integrity of buffer layer can potentially affect the fission-product retention. However, the average void size continuously decreases along the SiC radius in both locations.

Page intentionally left blank

CONTENTS

ABSTRACT.....	iv
ACRONYMS.....	x
1. Introduction.....	1
2. Experimental.....	2
2.1 Results and Discussion.....	2
SiC Grain Boundary Characterization	3
2.2 Comparison of Grain Boundary Distributions in Locations A & B.....	4
Grain Boundary Type.....	4
Grain Boundary Misorientation Angle.....	5
CSL Value.....	7
2.3 Chemical Analysis of Grain Boundary Fission Products.....	8
Comparison of Fission Products Type in Locations A & B.....	8
Fission Product and Grain Boundary Type	9
2.4 Comparison with Similar Safety-Tested AGR-1 Experiments	11
2.4.1 Grain Boundary Comparison	11
2.4.2 Fission-Product Comparison.....	13
2.5 Comparison with Non-Safety-Tested AGR-2 Particle.....	14
2.6 Irradiation Damage	16
3. Conclusions.....	19
4. Acknowledgement.....	19
5. References	20
Appendix A Detailed Quantitative Analysis of the SiC layer.....	21

FIGURES

Figure 1. (a) TEM analysis plan for AGR2-222-RS019, based on scanning electron microscopy (SEM) examination results. (b–c) Compilation of FIB-SEM images showing the three TEM lamella from the inner, center, and outer layer of SiC at Location A and Location B, respectively.	3
Figure 2. (a) A large view of the STEM dark field image taken from the Lamella 5 fabricated from the SiC/IPyC interface of Location B of the TRISO Particle AGR2-222-019. This image shows the areas of interests for STEM-EDS study. (b) The STEM image shows the detailed spots for EDS analysis on Area 2. (c) An <i>Image quality</i> micrograph generated by PED that shows the grain structures corresponding to Area 2. (d) Same <i>Image quality</i> micrograph with marked grain boundaries where spot chemical analysis were carried out. (e) The inverse pole figure shows the grain boundaries of interests.....	4
Figure 3. Plots showing the distribution of low angle, high angle and CSL grain boundaries for (a) each lamella and (b) the average of Location A and B of particle AGR2-222-RS019.....	5

Figure 4. Plots showing the distribution of grain boundary misorientation angles for (a) each lamella and (b) the average of Location A and B of particle AGR2-222-RS019.....	6
Figure 5. Plots showing the distribution of CSL values for (a) each lamella and (b) the average of Location A and B of particle AGR2-222-RS019.....	7
Figure 6. Distribution of fission products by compositions in AGR2-222-RS019.....	9
Figure 7. Distribution of fission products by grain boundary type in AGR2-222-RS019.....	10
Figure 8. Comparison of the SiC grain boundary types of AGR-1 and AGR-2 irradiated TRISO particles.....	12
Figure 9. Comparison of the SiC grain boundary misorientation angle of AGR-1 and AGR-2 irradiated TRISO particles.....	12
Figure 10. Comparison of the SiC grain boundary CSL value of AGR-1 and AGR-2 irradiated TRISO particles.....	13
Figure 11. Comparison of distribution of fission products by composition of AGR-1 and AGR-2 irradiated TRISO particles.....	13
Figure 12. Comparison of the SiC grain boundary types between safety-tested and non-safety-tested AGR-2 irradiated TRISO particles.....	14
Figure 13. Comparison of the SiC grain boundary misorientation angle between safety-tested and non-safety-tested AGR-2 irradiated TRISO particles.....	15
Figure 14. Comparison of the SiC grain boundary CSL values between safety-tested and non-safety-tested AGR-2 irradiated TRISO particles.....	16
Figure 15. The nature of the voids with sharp edges has been analyzed along the radial width of the SiC and is shown for the particle AGR2-222-RS019 for the inner (a, d), center (b, e) and outer (c, f) regions in Location A and B.....	17
Figure 16. The variation of void size along the radial distance of the SiC layer has been studied for Particle AGR2-222-RS019.....	18
Figure 17. A bright field TEM image shows the nonuniform distribution of irradiation damages in Lamella 5 of Location B. A similar observation has been made of all the lamella of Particle AGR2-222-RS019.....	18
Figure A1. (a) Large field of view STEM dark field image taken from the Lamella 1 fabricated from the SiC/IPyC interface of Location A on TRISO Particle AGR2-222-019. This image shows the areas of interests for the STEM-EDS study. STEM images on (b–d) show the detailed spots for EDS analysis on Area 1, 2, and 3, respectively.....	21
Figure A2. (a) Large field of view STEM dark field image taken from the Lamella 2 fabricated from the SiC/IPyC interface of Location A on TRISO Particle AGR2-222-019. This image shows the areas of interests for the STEM-EDS study. STEM images on (b–d) show the detailed spots for EDS analysis on Area 1, 2, and 3, respectively.....	23
Figure A3. (a) Large field of view STEM dark field image taken from the Lamella 3 fabricated from the SiC/IPyC interface of Location A of the TRISO Particle AGR2-222-019. This image shows the areas of interests for STEM-EDS study. STEM images on (b–d) shows the detailed spots for EDS analysis on Area 1, 2, and 3, respectively.....	25
Figure A4. (a) Large field of view STEM dark field image taken from the Lamella 5 fabricated from the SiC/IPyC interface of Location A on TRISO Particle AGR2-222-019. This	

image shows the areas of interests for STEM-EDS study. STEM images on (b–d) shows the detailed spots for EDS analysis on Area 1, 2, and 3, respectively.....	27
Figure A5. (a) Large field of view STEM dark field image taken from the Lamella 6 fabricated from the SiC/IPyC interface of Location A of the TRISO Particle AGR2-222-019. This image shows the areas of interests for STEM-EDS study. STEM images on (b-d) shows the detailed spots for EDS analysis on Area 1, 2, and 3, respectively.....	29
Figure A6. (a) Large field of view STEM dark field image taken from the Lamella 7 fabricated from the SiC/IPyC interface of Location A on TRISO Particle AGR2-222-019. This image shows the areas of interests for the STEM-EDS study. STEM images (b–d) show the detailed spots for EDS analysis on Area 1, 2, and 3, respectively.....	31

TABLES

Table 1. TRISO particle characteristics and average compact irradiation conditions (PS: pilot scale, TAVA: time average volume average, FIMA: fission per initial metal atom) [11]. Details of a specific AGR-1 particle have been provided for a comparative study.....	1
Table 2. Average fraction of grain boundary types in the SiC layer from Particle AGR2-222-019.....	5
Table 3. Average fraction of misorientation angles of grain boundaries in the SiC layer from Particle AGR2-222-019.....	6
Table 4. Average fraction of CSL types in the SiC layer from Particle AGR2-222-019.....	7
Table 5. Identification of precipitate types in Location A and B of SiC layer of particle AGR2-222-RS019.	9
Table 6. Relationship of grain boundaries nature and fraction of total precipitates in Location A and B of SiC layer of Particle AGR2-222-RS019.	10
Table A1. Qualitative EDS compositions from the SiC/IPyC interface of Location A from AGR2-222-019, taken from Areas 1, 2, and 3 that are highlighted in Figure A1.	22
Table A2. Qualitative EDS compositions from the center SiC layer of Location A from AGR2-222-019, taken from Areas 1, 2, and 3 that are highlighted in Figure A2.	23
Table A3. Qualitative EDS compositions from the outer SiC/OPyC layer of Location A from AGR2-222-019, taken from Areas 1,2 and 3 that are highlighted in Figure A3.	25
Table A4. Qualitative EDS compositions from the SiC/IPyC interface of Location B from AGR2-222-019, taken from Areas 1, 2, and 3 that are highlighted in Figure A4.	27
Table A5. Qualitative EDS compositions from the center SiC layer of Location B from AGR2-222-019, taken from Areas 1,2 and 3 that are highlighted in Figure A5.	29
Table A6. Qualitative EDS compositions from the outer SiC/OPyC layer of Location B from AGR2-222-019, taken from Areas 1 and 2 that are highlighted in Figure A6.	31

Page intentionally left blank

ACRONYMS

AGR	Advanced Gas Reactor
CSL	coincident site lattice
EDS	energy dispersive x-ray spectroscopy
FIB	focused ion beam
INL	Idaho National Laboratory
IPyC	inner pyrolytic carbon
OPyC	outer pyrolytic carbon
PED	precession electron diffraction
SEM	scanning electron microscopy
SiC	silicon carbide
STEM	scanning transmission electron microscopy
TEM	transmission electron microscopic
TRISO	tristructural isotropic

Page intentionally left blank

Electron Microscopic Examination of an Irradiated TRISO-Coated Particle of AGR-2 Experiment: AGR2-222-RS019

1. Introduction

The release of some metallic fission products from neutron-irradiated tristructural isotropic (TRISO) fuel particles, designed for advanced high-temperature nuclear reactors, has been regularly observed [1,2]. The silicon carbide (SiC) layer of the TRISO particle acts as the primary barrier for the containment of fission products. The advanced nanoscale investigation of TRISO particles, especially the SiC layer, reveals that the fission products react with SiC to form precipitates, with a range of compositions and sizes at the grain boundaries [3,4]. The transport mechanism of silver (^{110m}Ag) has been specifically important to the TRISO community, as the release of ^{110m}Ag is a potential worker safety concern due to plate-out on the cooler metallic parts of the helium pressure boundary. Along with that, specific fission products, such as palladium, can diffuse through both grain boundaries and the bulk SiC and form precipitates at grain boundaries as well as structural defects in the bulk SiC [5,6].

Previously, it has been observed that Pd can corrode SiC [7-9]. Significant SiC corrosion by Pd has NOT been observed except in some rare cases where there is thermomechanical cracking in the IPyC [10]. The reaction of Pd with SiC can potentially lead to the failure of TRISO particles at high burnup in low-enriched TRISO fuels when temperatures exceed 1100°C. Pd transport is also important, as the Ag transport has mostly been observed to be associated with Pd in SiC layer of a TRISO particle [9,11]; hence, it makes a compelling reason for the Pd transport study as well.

An earlier electron microscopic examination on the Idaho National Laboratory (INL) Advanced Gas Reactor 2 (AGR-2) TRISO coated particle AGR2-223-RS034 was completed [3,4] to identify fission-product precipitates along the grain boundaries of the SiC layer. This document presents the results obtained from the transmission electron microscopic (TEM) examination of an irradiated TRISO-coated particle from AGR-2 Compact 2-2-2. Compact 2-2-2 refers to the compact in Capsule 2 at Level 2 of Stack 2. The details of these particles are mentioned in Table 1. Details of an AGR-2 Compact 2-2-3 particle and two AGR-1 particles have been provided for a comparative study. The AGR-2 SiC was deposited using processes similar to the AGR-1 Variant 3 particles, of which two particles (AGR1-433-001 and AGR2-433-004) will be used for comparison. The AGR-1 coatings were produced on the lab-scale while the AGR-2 coatings were produced on the pilot or engineering scale. The AGR-1 and AGR-2 particles were safety tested at 1600°C.

Selected irradiation parameters and fuel properties are given in Table 1. For each fuel compact, physics calculations predicted the amount of fission-product silver produced in an average fuel particle. The “Ag Retention” column is the ratio of the Ag content of the specific particle measured during post-irradiation examinations compared to the physics prediction [12-14]. Ag release is used as a metric for fuel performance. The burnup, fluence, and temperatures are calculated values averaged over the specific compact. Individual particle irradiation conditions may vary from the average [15]. It is reasonable to expect that particles from compacts that were safety tested would have different Ag retention than otherwise identical particles that were not safety tested.

Table 1. Characteristics and average compact irradiation conditions for particle AGR2-222-RS019 (TAVA: time average volume average, FIMA: fission per initial metal atom) [15].

Particle	Particle Ag Retention (%)	Irradiation Properties Averaged Over the Entire Compact. Actual particle properties will vary.			
		Burnup (%FIMA)	Fast Neutron Fluence, $\times 10^{25}$ n/m ²	TAVA Temp (°C)	Time-Ave Peak Temp (°C)
AGR2-222-RS019 (Safety Tested)	20	12.55	3.39	1287	1354
AGR2-223-RS034	84	10.8	2.99	1161	1335
AGR1-433-001 (Safety Tested)	66	18.6	4.16	1094	1179
AGR1-433-004 (Safety Tested)	98	18.6	4.16	1094	1179

While the micron-scale fission-product precipitates in the SiC and inner pyrolytic carbon (IPyC) layers are found to be formed of different chemically segregated regions [16], this report focuses on the SiC grain boundary precipitate compositions and their relationship with grain boundary nature. This report presents the results from scanning transmission electron microscopy (STEM), STEM–energy dispersive spectrometry (EDS), and precision electron diffraction (PED) obtained from an irradiated AGR2-222-RS019 particle. The irradiation defects character has been determined through TEM imaging, using void size and their radial variation along the SiC layer.

2. Experimental Design

TRISO-coated nuclear fuel was fabricated using an engineering-scale process and was subjected to irradiation under the AGR-2 experimental programs in the Advanced Test Reactor at INL. Following irradiation, the AGR-2 fuel compact was electrolytically deconsolidated. The AGR2-222-RS019 particle from the compact was examined using a set of advanced microscopic techniques.

Samples for the TEM were prepared by a dual-beam Quanta 3D focused ion beam (FIB) instrument. To minimize the possible Ga ion damage, the TEM samples were cleaned using 5kV and a current of ~50 pA for 2–5 minutes per side. STEM and conventional TEM imaging were conducted on an FEI Tecnai F30 microscope operated at 300 kV. An electron probe size of 5 nm, in conjunction with a 4-nm step size, was used to collect crystallographic orientation data. The crystallographic information was exported and analyzed using EDAX OIM v7.1.0 software. Two data cleanup routines were applied to all data and resulted in less than 3% of the data points being affected, well below the limit of 10% that is allowed in Section 12.2 of the American Society for Testing and Materials Standard E2627 [17]. Grain boundaries were defined for a misorientation greater than or equal to 2°. The range of coincident site lattice (CSL)-related grain boundaries was defined to include $\Sigma 3$ through $\Sigma 29$. Chemical analyses on the TEM samples were carried out using the EDAX EDS system. Gatan digital micrograph and the TEM imaging and analysis software were used for post-processing of TEM data.

2.1 Results and Discussion

The TEM analysis plan for AGR2-222-RS019, shown in Figure 1(a), shows that Location A was selected from a region in the SiC layer where there was less of a gap between the buffer and IPyC layers while Location B was selected in a region where there was a significant gap between the buffer and IPyC layers. However, the IPyC/SiC interface was intact in both locations (no gap between these two layers). Figure 1(b–c) shows the TEM lamella prepared using the FIB in three areas (IPyC/SiC interface, SiC, and SiC/Outer pyrolytic carbon (OPyC) interface) in both Locations A and B, respectively.

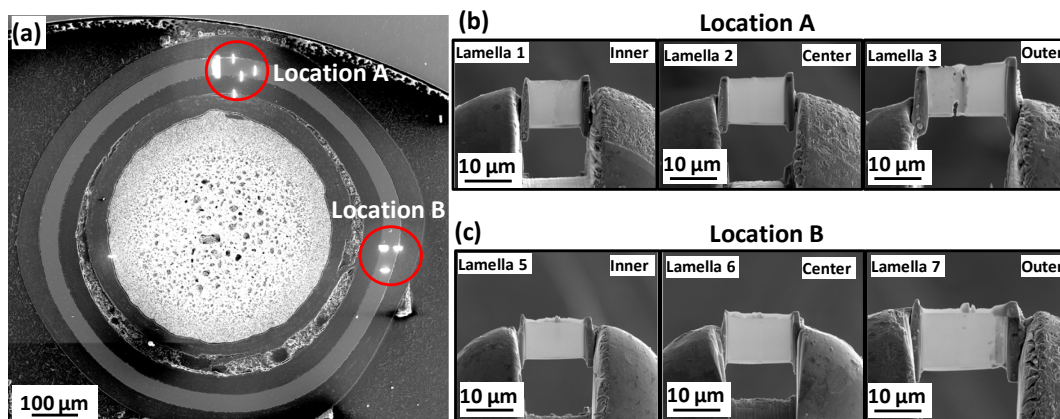


Figure 1. (a) TEM analysis plan for AGR2-222-RS019, based on scanning electron microscopy (SEM) examination results. (b–c) Compilation of FIB-SEM images showing the three TEM lamella from the inner, center, and outer layer of SiC at Location A and Location B, respectively.

SiC Grain Boundary Characterization

Previously, we have observed that the nature of grain boundaries influences the precipitation of fission products on them. Hence, the SiC grain boundaries have been characterized by PED in detail to show the distribution of low-angle, high-angle, and CSL grain boundaries and the association to fission-product precipitates. Further, the variation of grain boundaries along the radial length (i.e., in the three layers designated in this study as in IPyC/SiC, SiC and SiC/OPyC layer) has been analyzed.

Figure 2 shows the coupling the TEM-EDS and PED for associating the grain boundary nature and compositions of fission products. For a representation of this approach, see Figure 2(a-b), which shows the STEM image of Lamellae 5 and a selected Area 2 for the analysis, respectively. Figure 2(c–e) show the orientation mapping images that correspond to the same Area-2 where the EDS quantification of grain boundary precipitates was performed. All three lamella of both Locations A and B are analyzed at three different locations in similar fashion.

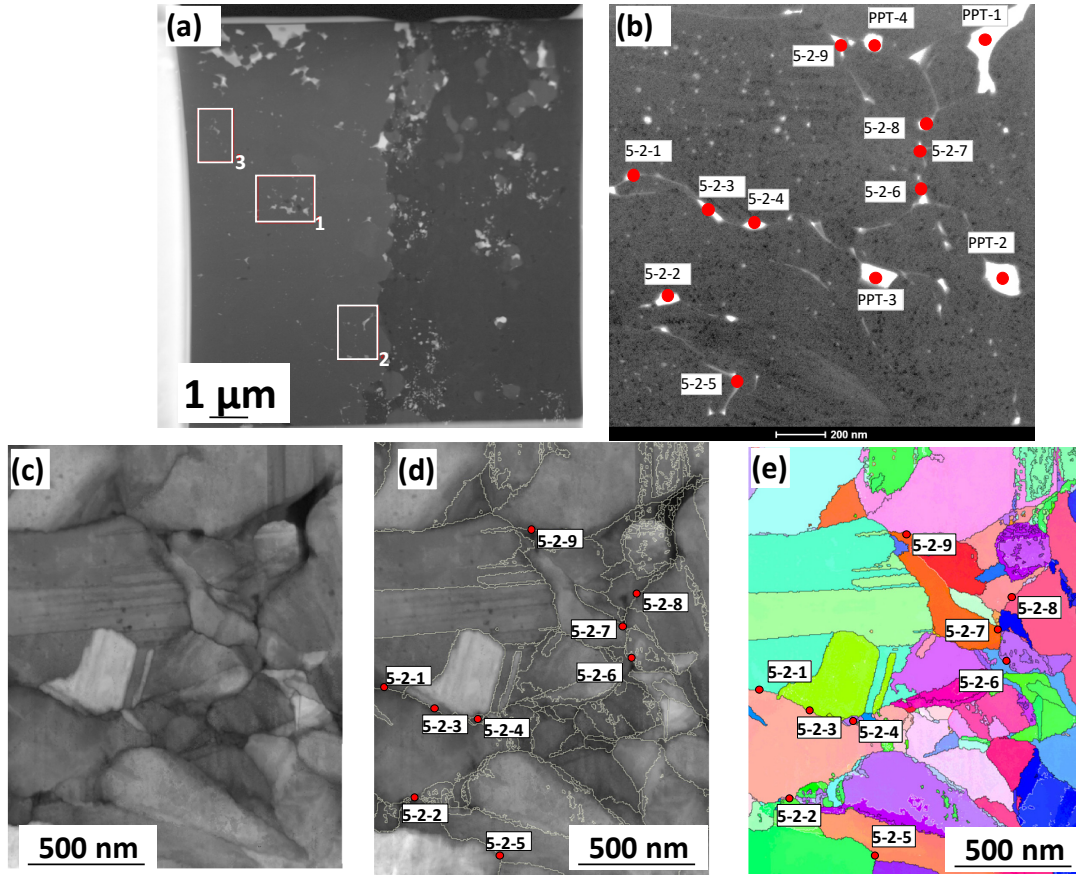


Figure 2. (a) A large view of the STEM dark field image taken from the Lamella 5 fabricated from the SiC/IPyC interface of Location B of the TRISO Particle AGR2-222-019. This image shows the areas of interests for STEM-EDS study. (b) The STEM image shows the detailed spots for EDS analysis on Area 2. (c) An *Image quality* micrograph generated by PED that shows the grain structures corresponding to Area 2. (d) The same *Image quality* micrograph with marked grain boundaries where spot chemical analysis was carried out. (e) The inverse pole figure shows the grain boundaries of interests.

2.2 Comparison of Grain Boundary Distributions in Locations A & B

Grain Boundary Type

The grain boundary distributions associated with inner, center, and outer regions of the SiC layer at Locations A and B are shown in Figure 3. Figure 3(a–b) shows there are no statistical difference in the distributions of grain boundary type across the SiC layer in Location A and B. Table 2 quantifies the average fractions of the grain boundary type for Location A and B. From Figure 3 (b), Location A has slightly higher low-angle and high-angle grain boundaries than those in Locations B. Also, Location B has higher CSL-related grain boundaries compared to Location A, as shown in Figure 3 (b).

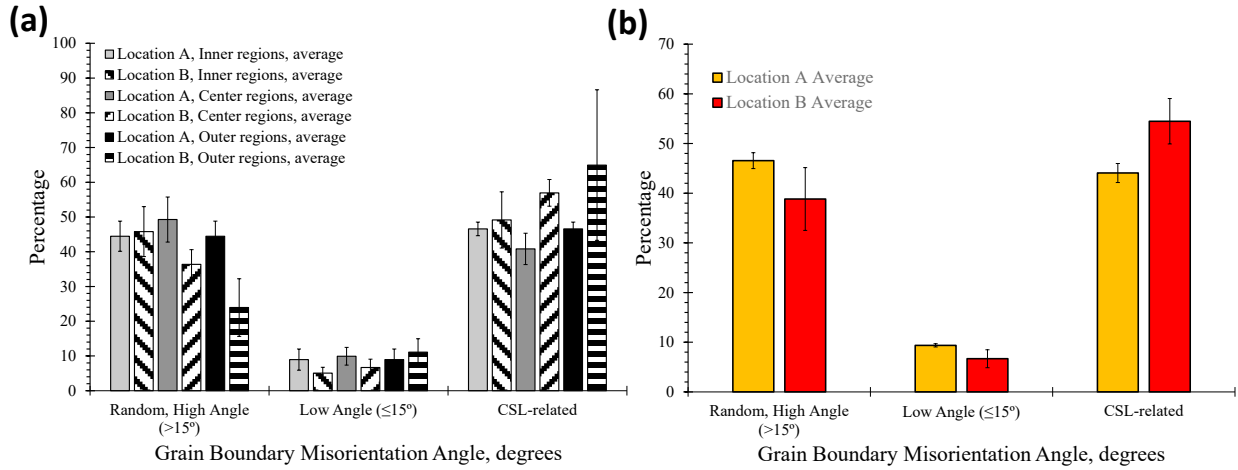


Figure 3. Plots showing the distribution of low-angle, high-angle and CSL grain boundaries for (a) each lamella and (b) the average of Location A and B of particle AGR2-222-RS019.

Table 2. Average fraction of grain boundary types in the SiC layer from Particle AGR2-222-019.

Grain Boundary Type	Fraction, %	Standard Error
Location A		
Random, High Angle (>15°)	46.6	1.6
Low Angle (≤15°)	9.4	0.3
CSL-related	44.1	1.9
Location B		
Random, High Angle (>15°)	38.8	6.3
Low Angle (≤15°)	6.7	1.8
CSL-related	54.5	4.6

Grain Boundary Misorientation Angle

Figure 4 shows the determination of the grain boundary distribution in each area analyzed in Location A and B. The distributions of grain boundary misorientation angles found in each area and the average distribution are given in Figure 4(a–b), respectively. Table 3 quantifies the average fractions of grain boundary misorientation angles for Location A and B.

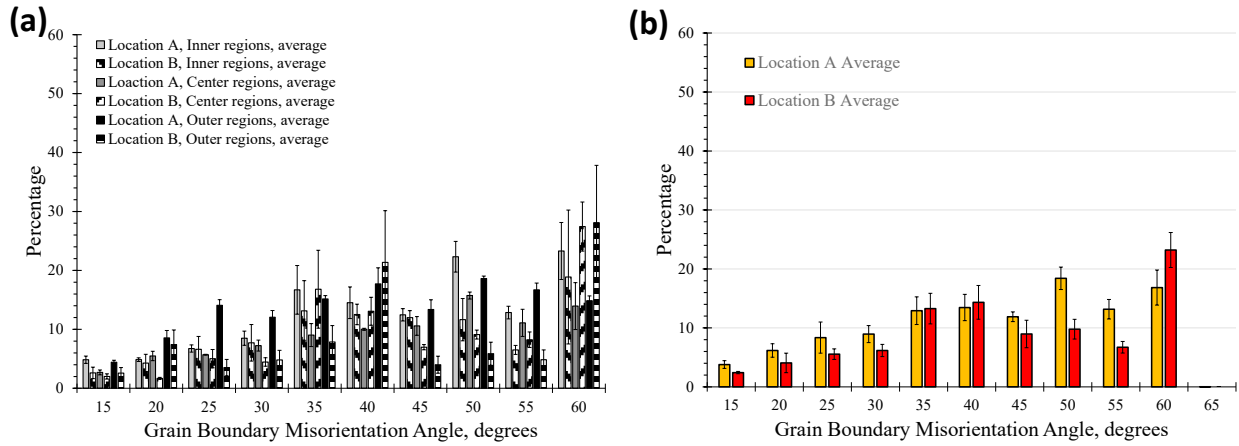


Figure 4. Plots showing the distribution of grain boundary misorientation angles for (a) each lamella and (b) the average of Location A and B of particle AGR2-222-RS019.

Table 3. Average fraction of misorientation angles of grain boundaries in the SiC layer from Particle AGR2-222-019.

Location A Average	Misorientation Angle, degrees	Fraction, %	Std. Error
	15	2.4	0.7
	20	4.1	1.1
	25	5.6	2.6
	30	6.2	1.4
	35	13.3	2.3
	40	14.3	2.2
	45	9.0	0.8
	50	9.8	1.9
	55	6.7	1.7
	60	23.2	3.0
	65	0.0	0.0

Location B Average	Misorientation Angle, degrees	Fraction, %	Std. Error
	15	2.4	0.2
	20	4.1	1.7
	25	5.6	0.9
	30	6.2	1.0
	35	13.3	2.6
	40	14.3	2.9
	45	9.0	2.3
	50	9.8	1.7
	55	6.7	1.0
	60	23.2	3.0
	65	0.0	0.0

CSL Value

Figure 5 shows the distribution of the CSL value in each area analyzed in Location A and B. The distributions of CSL value found in each area and the average distribution are given in Figure 5(a-b), respectively. Table 4 quantifies the average fractions of grain boundary misorientation angles for Location A and B.

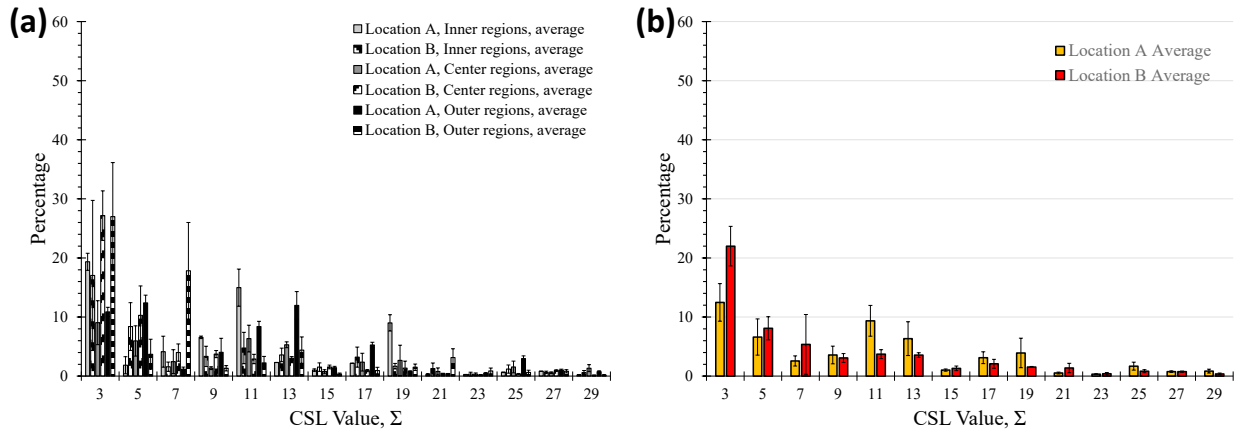


Figure 5. Plots showing the distribution of CSL values for (a) each lamella and (b) the average of Location A and B of particle AGR2-222-RS019.

Table 4. Average fraction of CSL types in the SiC layer from Particle AGR2-222-019.

CSL Value, Σ	Number of Boundaries	Fraction, %	Std. Error
Location A			
3	24,181	12.5	3.2
5	12,817	6.6	3.1
7	4,974	2.6	0.9
9	6,937	3.6	1.5
11	18,150	9.4	2.6

CSL Value, Σ	Number of Boundaries	Fraction, %	Std. Error
13	12,295	6.3	2.9
15	1,997	1.0	0.2
17	6,054	3.1	1.0
19	7,603	3.9	2.5
21	1,019	0.5	0.2
23	653	0.3	0.1
25	3,271	1.7	0.7
27	1,482	0.8	0.1
29	1,646	0.8	0.3
Location B			
3	29,931	22.0	3.3
5	11,010	8.1	2.0
7	7,299	5.4	5.1
9	4,188	3.1	0.7
11	5,055	3.7	0.8
13	4,852	3.6	0.4
15	1,789	1.3	0.4
17	2,843	2.1	0.8
19	2,107	1.5	0.1
21	1,867	1.4	0.8
23	545	0.4	0.2
25	1,128	0.8	0.2
27	1,035	0.8	0.1
29	501	0.4	0.2

2.3 Chemical Analysis of Grain Boundary Fission Products

Comparison of Fission Products Type in Locations A & B

The chemistry of fission-product precipitates at the SiC grain boundaries and triple junctions are documented in this section of the report. The detailed quantification of each spot EDS from all lamella are provided in Appendix A. Table 5 mentions the basic constituents of all fission-product precipitates observed in Locations A and B. The grain boundary precipitates are mostly observed to be silicide compounds from previous studies [6,13]. From Table 5, Ag is observed at only the IPyC/SiC layer, and it is collocated with Pd. This table indicates that the compositional complexity of fission-product precipitates decreases along the outward radial distance of SiC. However, Pd appears to be the only fission product present in sufficiently high quantities that these methods can detect its presence in the SiC in both Location A and B.

Table 5. Identification of precipitate types in Location A and B of SiC layer of particle AGR2-222-RS019.

			Precipitates
Location A		Lamella 1 - Inner Area	Pd, Pd-Ag, Pd-U, Pd-Pu
		Lamella 2 - Center Area	Pd, Pd-Pu
		Lamella 3 - Outer Area	Pd
Location B		Lamella 5 - Inner Area	Pd, Pd-U, Pd-Pu
		Lamella 6 - Center Area	Pd, Pd-Pu
		Lamella 7 - Outer Area	Pd, Pd-Pu

Figure 6 shows the distribution of fission products by composition in both Location A and B. IT is observed that the Location A (adjacent to intact buffer) has significantly more Pd-containing fission products compared to Location B (adjacent to broken buffer layer).

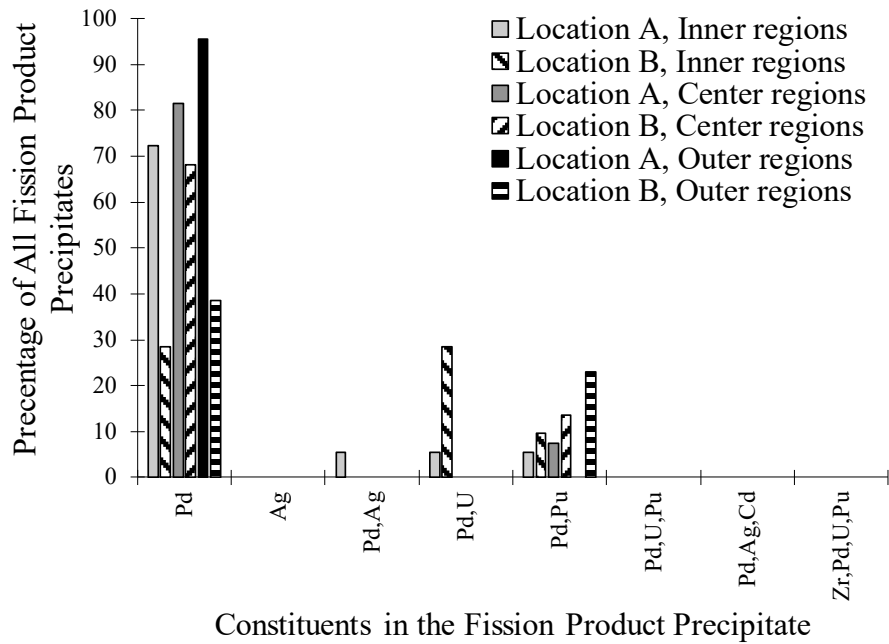


Figure 6. Distribution of fission products by compositions in AGR2-222-RS019.

Fission Product and Grain Boundary Type

Figure 7 shows the distribution of fission products by composition in both Location A and B. There is no significant difference in fission-product precipitation due to grain boundary nature in either location. Table 6 mentions the distribution of fission-product precipitates according to the grain boundary nature. One of the observations is the precipitation at low-angle grain boundaries in both locations.

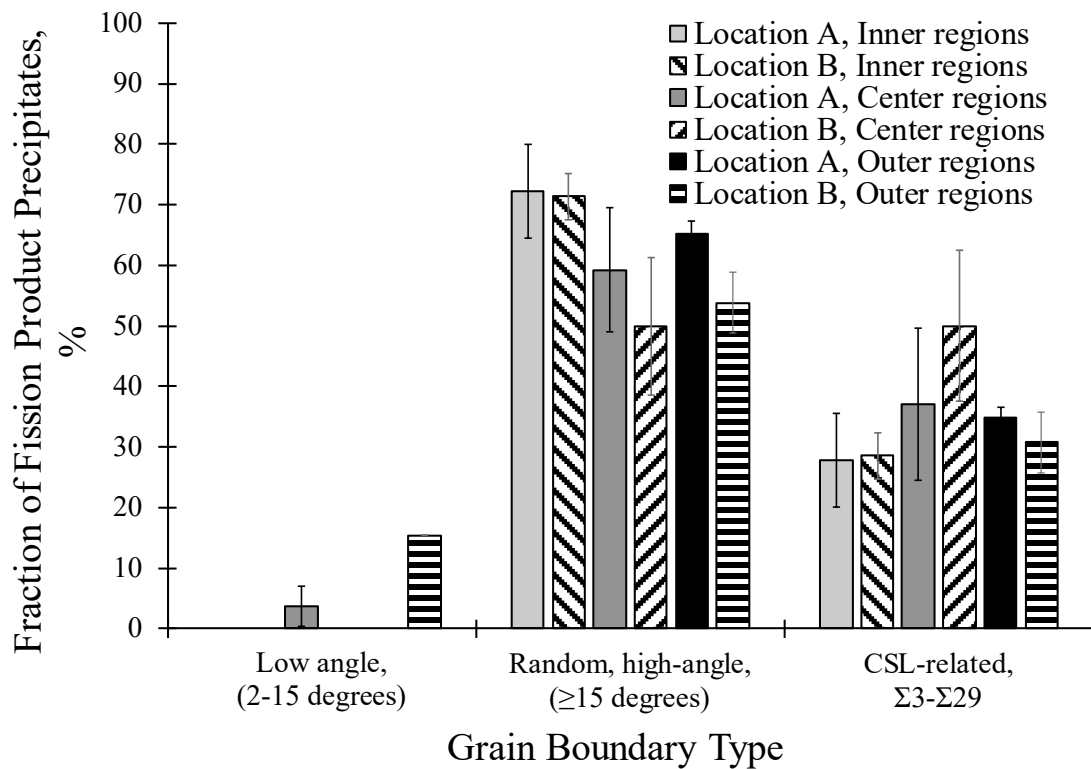


Figure 7. Distribution of fission products by grain boundary type in AGR2-222-RS019.

Table 6. Relationship of grain boundaries nature and fraction of total precipitates in Location A and B of SiC layer of Particle AGR2-222-RS019. Location A contains Lamella 1-3, and Location B contains Lamella 5-7.

	Boundary type	Fraction, %	Std. error
Lamellae 1	Low angle	0	0.0
	High angle - not CSL	72	7.7
	CSL	28	7.7
Lamellae 2	Low angle	4	3.3
	High angle - not CSL	59	10.3
	CSL	37	12.5
Lamellae 3	Low angle	0	3.1
	High angle - not CSL	65	2.2
	CSL	35	1.8
Location A average	Low angle	1.5	1.2
	High angle - not CSL	64.7	3.7
	CSL	33.8	2.8

	Boundary type	Fraction, %	Std. error
Lamellae 5	Low angle	0	0.0
	High angle - not CSL	71	3.8
	CSL	29	3.8
Lamellae 6	Low angle	0	23.7
	High angle - not CSL	50	11.4
	CSL	50	12.5
Lamellae 7	Low angle	15	0.0
	High angle - not CSL	54	5.0
	CSL	31	5.0
Location B average	Low angle	3.6	5.1
	High angle - not CSL	58.9	6.6
	CSL	37.5	6.8

2.4 Comparison with Similar Safety-Tested AGR-1 Experiments

While the TRISO particles for AGR-2 experiments were fabricated at pilot scale, the particles in the AGR-1 experiments were fabricated at laboratory scale. The AGR-2 TRISO fuel particles were fabricated using conditions very similar to those used to fabricate AGR-1, Variant 3 TRISO fuel particles. Hence, a direct comparison of AGR-2 and AGR-1, Variant 3 irradiated TRISO particles is of interest to check the details of fission product transport in SiC layer. In this section, the advanced microscopy results from the safety-tested AGR2-222-RS019 particle will be compared with similar safety-tested AGR1-433-001 and AGR1-433-004 particles. The Ag retention in AGR1-433-001 and AGR2-433-004 particles are 66% and 98%, respectively. Additionally, the grain boundary information of the AGR2-222-RS019 particle will be compared with that of a non-safety-tested AGR2-223-RS034 particle with an 84% Ag retention.

2.4.1 Grain Boundary Comparison

Figure 8 plots the comparison of the average grain boundary distributions for Particle AGR2-222-RS019 with AGR-1, Variant 3 particles (AGR1-433-001 and AGR1-433-004) that have been previously analyzed with similar methods. From this plot, it appears that the AGR-2 particle has a significantly higher percentage of high-angle grain boundaries. As high-angle grain boundaries are more preferred paths for fission product transport due to higher grain boundary energy, the AGR-2 particle may contain a larger amount of fission products at the grain boundary as compared to these AGR-1 particles.

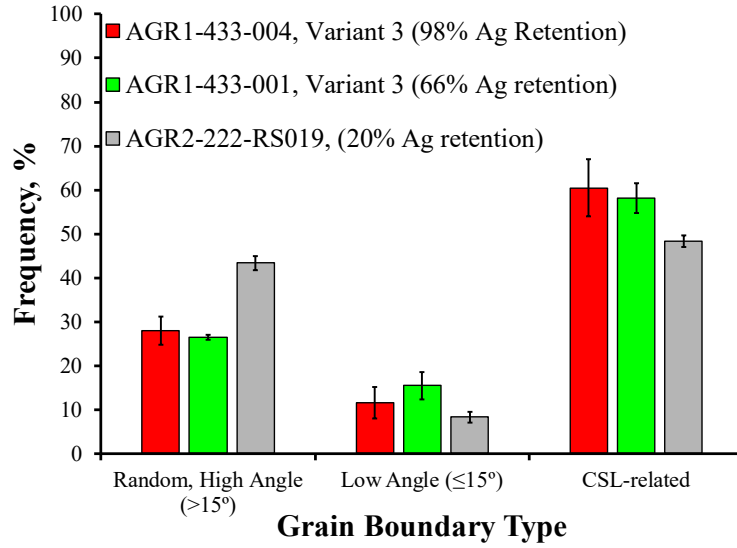


Figure 8. Comparison of the SiC grain boundary types of AGR-1 and AGR-2 irradiated TRISO particles.

Figure 9 shows the details of the comparison of the SiC grain boundary misorientation angle among these safety-tested AGR-1 and AGR-2 particles. Figure 9 shows that the fraction of various misorientation angle in AGR-2 particle is roughly uniform. But the misorientation angle of 60° in AGR-1 particles is very high. Previous analyses on other variants of AGR-1 particles concluded that irradiation does not significantly alter the SiC microstructure [18]. These variations appear to indicate that inherent variation arises during fabrication.

Similarly, Figure 10 shows the comparison of CSL grain boundary values among these AGR-1 and AGR-2 particles. A low twin percentage (misorientation angle of 60°) is found in AGR-2 particles compared to AGR-1 particles. As the fabrication methods of AGR-1 and AGR-2 particles are very similar, the variation in twin fraction possibly arises from lack of a large statistical sampling of SiC layer.

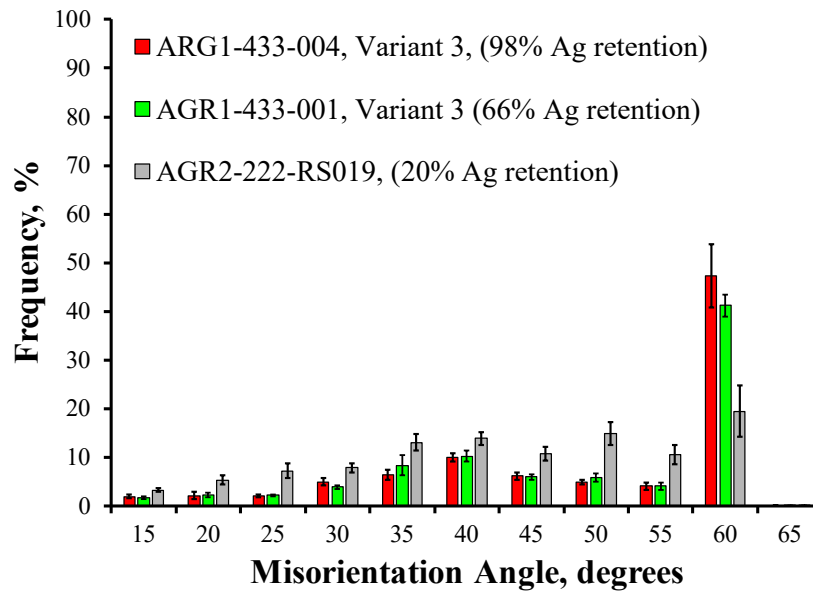


Figure 9. Comparison of the SiC grain boundary misorientation angle of AGR-1 and AGR-2 irradiated TRISO particles.

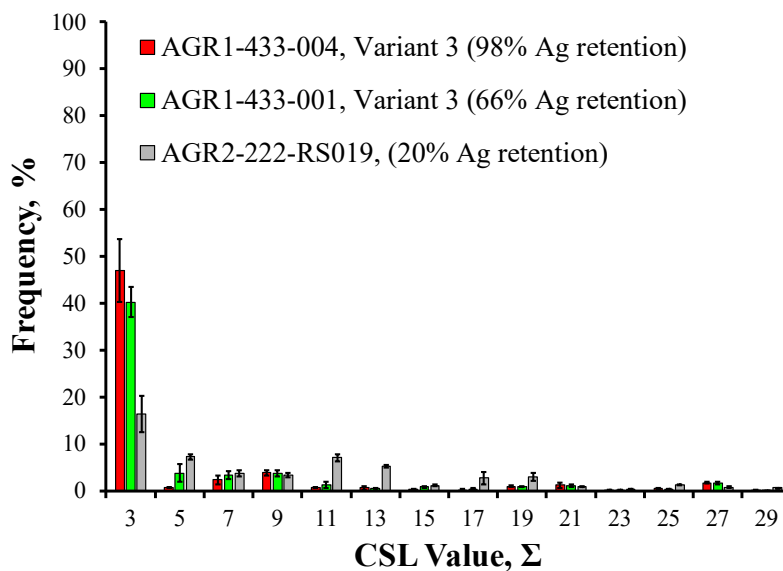


Figure 10. Comparison of the SiC grain boundary CSL value of AGR-1 and AGR-2 irradiated TRISO particles.

2.4.2 Fission-Product Comparison

Figure 11 shows the distribution of fission products by their compositional nature in AGR-1 and AGR-2 particles. It is worth noticing that only AGR-1 particles were observed to contain fission-product precipitates with “only Ag.”

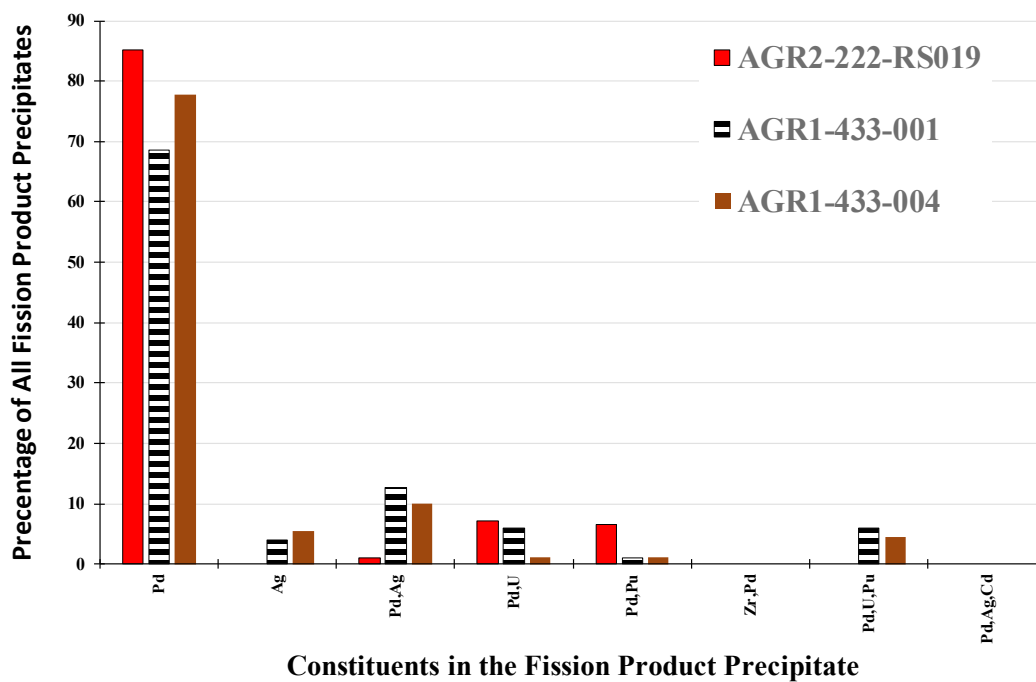


Figure 11. Comparison of distribution of fission products by composition of AGR-1 and AGR-2 irradiated TRISO particles.

2.5 Comparison with Non-Safety-Tested AGR-2 Particle

Figure 12 plots a comparison of the average grain boundary distributions for safety tested AGR2-222-RS019 with the non-safety-tested AGR2-223-RS034. From this plot, it appears that AGR2-222-RS019 has a slightly higher percentage of high-angle grain boundaries. As a high-angle grain boundary is the most preferred path for fission product transport, AGR-2 particles may contain larger amounts of fission products at grain boundaries as compared to this specific non-safety-tested AGR-2 particle.

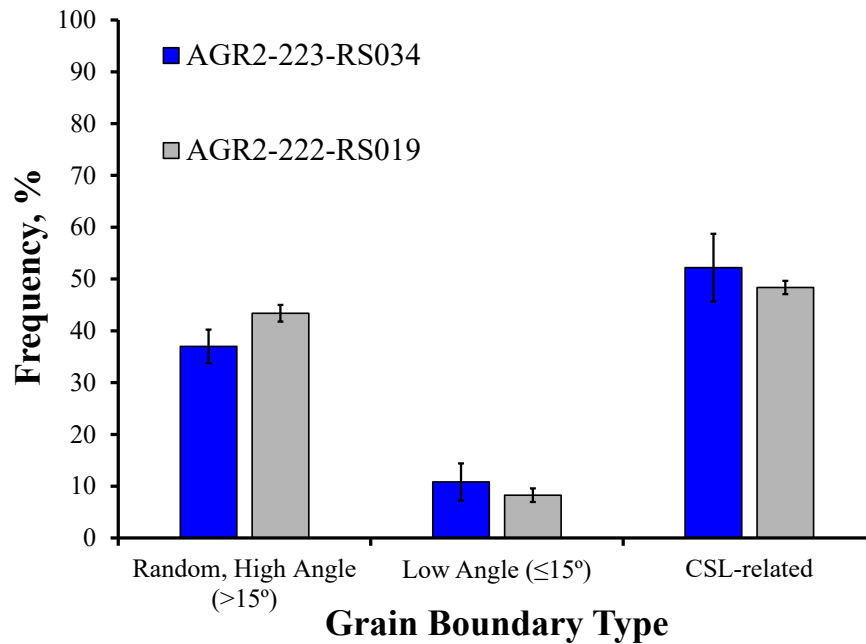


Figure 12. Comparison of the SiC grain boundary types between safety-tested and non-safety-tested AGR-2 irradiated TRISO particles.

Figure 13 shows details of a comparison of the SiC grain boundary misorientation angle between these two AGR-2 particles. The plot reveals that the non-safety tested AGR2 particle has the highest misorientation angle of 60°. This variation appears to indicate that inherent variation can arise during the fabrication method. Previous analyses on other variants of AGR-1 and AGR-2 particles have concluded that irradiation has little effect on the as-fabricated SiC microstructure.

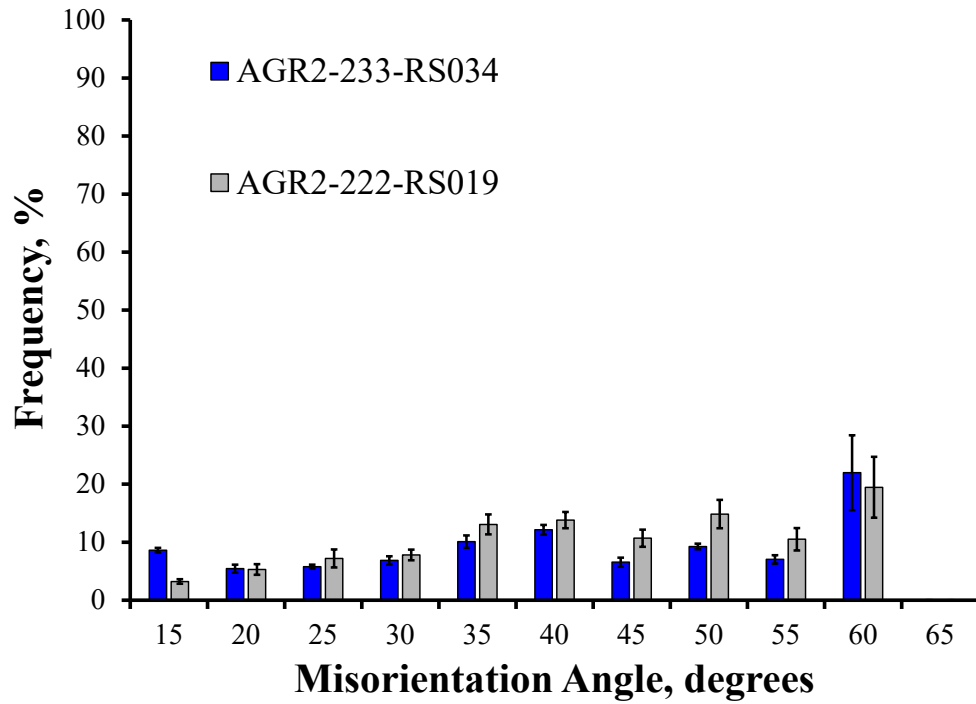


Figure 13. Comparison of the SiC grain boundary misorientation angle between safety-tested and non-safety-tested AGR-2 irradiated TRISO particles.

Figure 14 shows a comparison of CSL grain boundary values between these AGR-2 particles. Both particles have a similar twin grain boundary percentage.

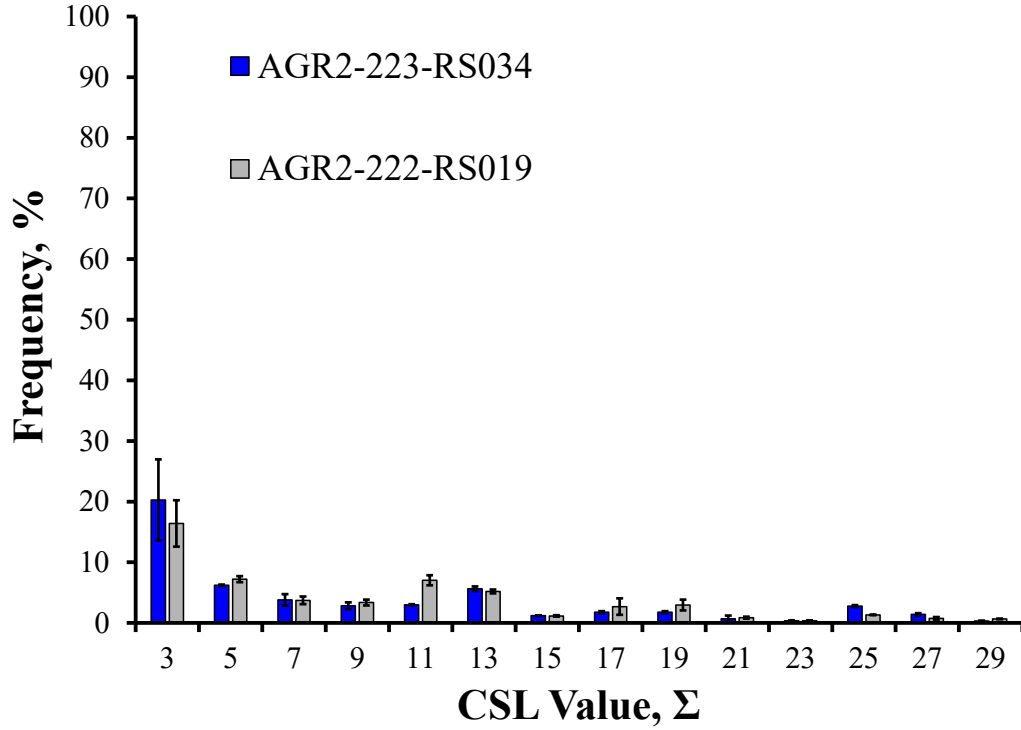


Figure 14. Comparison of the SiC grain boundary CSL values between safety-tested and non-safety-tested AGR-2 irradiated TRISO particles.

2.6 Irradiation Damage

Neutron-irradiation damage structures are expected to accelerate the intragranular diffusion kinetics of fission products [19,20]. Hence, their size, shape, and distribution patterns across the radial thickness of the SiC layer can be directly correlated with the nature of intragranular transport pathways of fission products. Figure 15 shows the TEM bright field images that shows the distribution, shape, and size of irradiation damages. The damages have tetragonal shape. The details of the crystallographic orientation have been previously reported by van Rooyen et al. [19]. TEM imaging was carried out either in overfocus or underfocus bright field conditions for the better visibility of the defect structures.

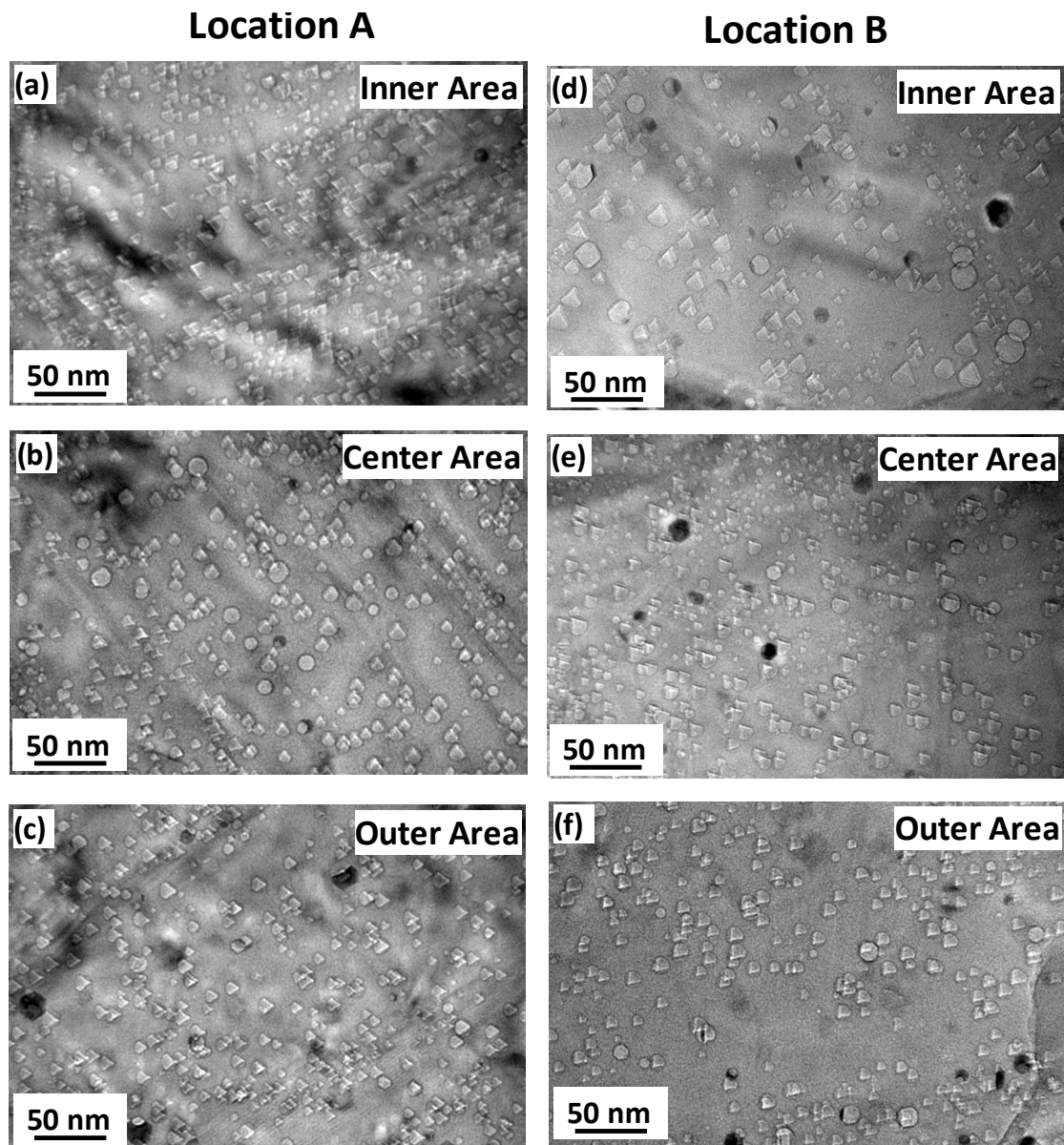


Figure 15. The nature of the voids with sharp edges has been analyzed along the radial width of the SiC and is shown for the particle AGR2-222-RS019 for the inner (a, d), center (b, e) and outer (c, f) regions in Location A and B. Locations A (near intact buffer-IPyC bonding) and B (where the buffer is no longer bonded to the IPyC).

Figure 16 shows the variation in the size of voids along the radial distance of SiC. The analysis on two locations (A and B) shows a larger void in the inner region at Location B where there is a breakage in the buffer region. As the neutron flux can be assumed to be the same at all parts in the particle, the larger void size at Location B might indicate that the Location B was subjected to higher temperature. Moreover, A general decrease in void size across the radius of the SiC, as observed in Figure 16, could be indicative of the temperature gradient decreasing from the inside out.

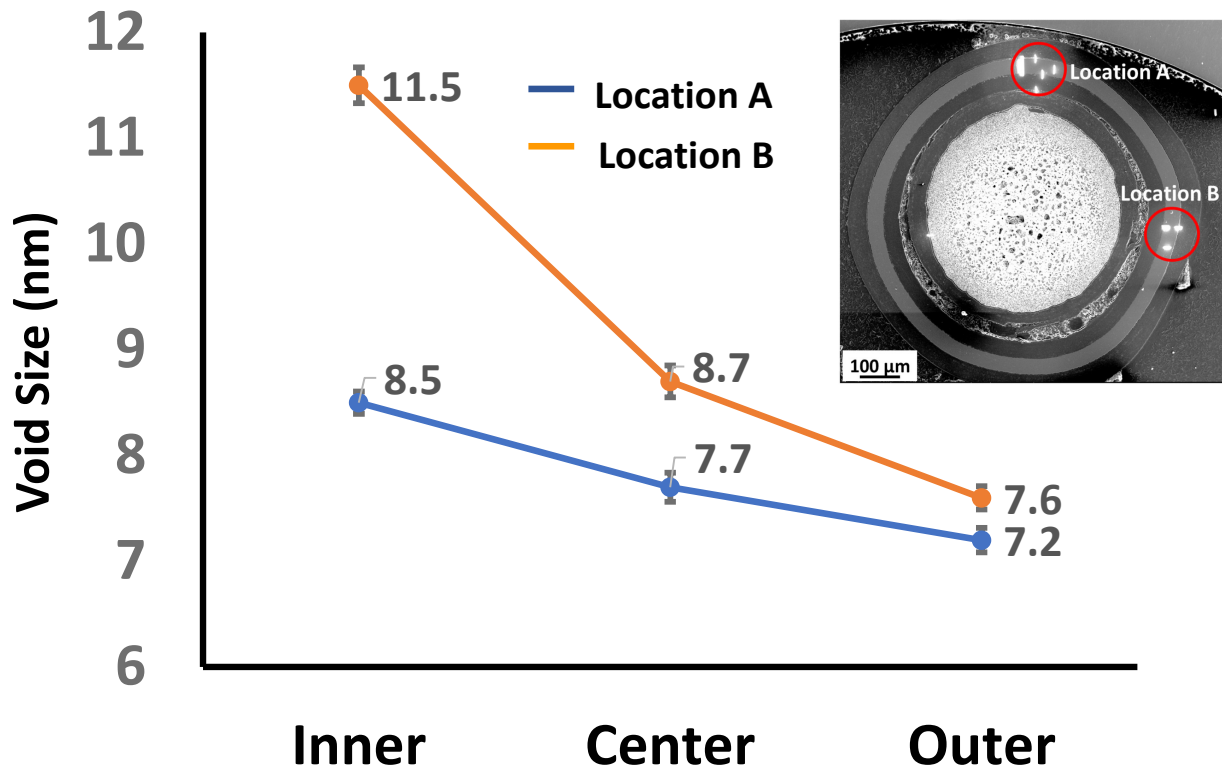


Figure 16. The variation of void size along the radial distance of the SiC layer has been studied for Particle AGR2-222-RS019.

We also observed that the voids near stacking faults are aligned along the length of the faults. It is expected that preferential void nucleation has occurred at these stacking faults. The nanoscale intragranular precipitates (mostly Pd rich [6]) appear to be confined between a pair of stacking faults, as evident from the segregation of neutron-irradiation damage to the stacking faults seen in Figure 17.

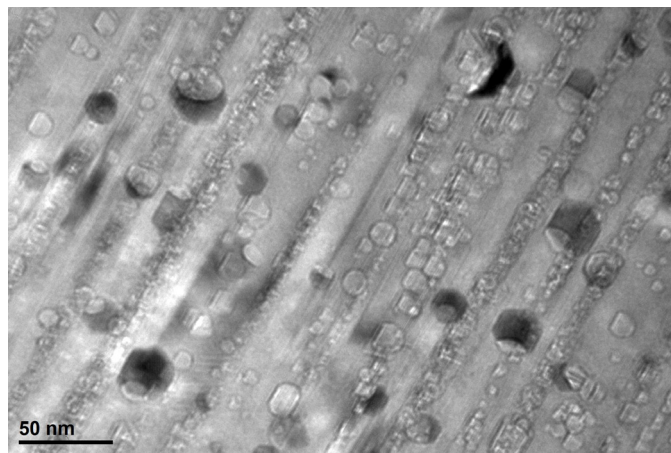


Figure 17. A bright field TEM image shows the non-uniform distribution of irradiation damages in Lamella 5 of Location B. A similar observation has been made of all the lamella of Particle AGR2-222-RS019.

3. Conclusions

This electron microscopy study on fission-product transport phenomena in the SiC layer of neutron-irradiated TRISO fuel in an AGR2-222-RS019 particle can be summarized as follows:

- Most fission product precipitates were associated with random, high-angle grain boundaries, although precipitates were found on grain boundaries with a CSL relationship to a lesser degree.
- Pd was the fission-product element found most often in the precipitates, although a few precipitates containing Ag, Cd, Zr, and Mo (in various combinations) were also found. See Appendix A.
- The compositional complexity of fission-product precipitates decreases towards the outer layer of SiC.
- A comparison of the results to previously irradiated and analyzed, Variant 3, safety-tested AGR-1 TRISO particles showed that the grain boundary distributions have some minor differences. The differences in CSL grain boundary and misorientation angles are possibly inherent to the fabrication process.
- A general decrease in void size across the radius of the SiC can be indicative of the temperature gradient decreasing from the inside out.

4. Acknowledgement

This work was sponsored by the U.S. Department of Energy, Office of Nuclear Energy, under U.S. Department of Energy Idaho Operations Office Contract DE-AC07-05ID14517, as part of the Advanced Reactor Development Program. The United States Government retains and the publisher, by accepting the article for publication, acknowledges that the United States Government retains a nonexclusive, paid-up, irrevocable, world-wide license to publish or reproduce the published form of this manuscript, or allow others to do so, for United States Government purposes. The authors would like to acknowledge the efforts of Mr. James Madden in the FIB fabrication of the TEM samples as well as staff at the Materials and Fuels Complex at INL. TEM work was carried out at the Center for Advanced Energy Studies Microscopy and Characterization Suite.

5. References

- [1] H. Nabielek, P.E. Brown, P. Offerman, Nucl. Technol., 35 (1977), p. 48
- [2] P.A. Demkowicz et al, Preliminary results of post-irradiation examination of the AGR-1 TRISO fuel compacts, Paper HTR2012-3-021, in: Proceedings of the HTR 2012, Tokyo, Japan, October 28–November 1, 2012.
- [3] I.J. van Rooyen, T.M. Lillo, Y.Q. Wu, Journal of Nuclear Materials, 446 (2014) 178-186.
- [4] T.M. Lillo, I.J. Van Rooyen, Journal of Nuclear Materials, 460 (2015) 97-106.
- [5] S. Meher, I.J. van Rooyen, C. Jiang, Journal of Nuclear Materials, 527 (2019) 151793.
- [6] S. Meher, I.J. van Rooyen, T.M. Lillo, Scientific Reports, 8, (2018) 98.
- [7] M. Barrachin, R. Dubourg, S. De Groot, M.P. Kissane, K. Bakker, J. Nucl. Mater., 415 (2011), pp. 104-116
- [8] K. Minato, T. Ogawa, K. Fakuda, H. Sekino, H. Miyanishi, S. Kado, I. Takahashi, J. Nucl. Mater., 202 (1993), pp. 47-53
- [9] P. Demkowicz, K. Wright, J. Gan, D. Petti, Solid State Ionics, 179 (39) (2008), pp. 2313-2321
- [10] J. D. Hunn, C. A. Baldwin, T. J. Gerczak, F. C. Montgomery, R. N. Morris, C. M. Silva, P. A. Demkowicz, J. M. Harp, S. A. Ploger, Detection and analysis of particles with failed SiC in AGR-1 fuel compacts, Nuc. Eng. Design, 306 (2016) 36-46.
- [11] J. Neethling, J. O’Connell, J. Olivier, Palladium assisted silver transport in polycrystalline SiC, AG-PD HTR2010-196.
- [12] J.D. Hunn, C.A. Baldwin, T.J. Gerczak, et al. AGR-1 Irradiated Compacts 5-2-3 and 5-2-1 PIE Report: Evaluation of As-Irradiated Fuel Performance with Leach-Burn-Leach, IMGA, Materialography, and X-Ray Tomography, Oak Ridge National Laboratory (2014), ORNL/TM-2014/171
- [13] J.D. Hunn, C.A. Baldwin, F.C. Montgomery, T.J. Gerczak, R.N. Morris, G.W. Helmreich, P.A. Demkowicz, J.M. Harp, J.D. Stempien, Initial examination of fuel compacts and TRISO particles from the US AGR-2 irradiation test, Nucl. Eng. Des., 329 (2018), pp. 89-101.
- [14] P. Demkowicz, J. Harp, P. Winston, S. Ploger, AGR-1 Fuel Compact 6-3-2 Post-Irradiation Examination Results, Idaho National Laboratory (2012) INL/EXT-12-27123
- [15] B.P. Collin, AGR-2 Irradiation Test Final As-Run Report, INL/EXT-14-32277, rev. 2, August 2014.
- [16] S. Meher, I.J. van Rooyen, C. Jiang, Journal of Nuclear Materials Volume 527 (2019), 151793.
- [17] ASTM Standard E2627-13, “Standard Practice for Determining Average Grain Size Using Electron Backscatter Diffraction (EBSD) in Fully Recrystallized Polycrystalline Materials.”, ASTM International, West Conshohocken, PA, 2013, www.astm.org.
- [18] T.M. Lillo, I.J. van Rooyen, J.A. Aguiar, Nuc. Eng. Design 329, (2018) 46-52.
- [19] I.J. van Rooyen, S. Meher, J. Rosales Proceedings of HTR (2018), Paper No. 3013.
- [20] S. Kondo, Y. Katoh, L. Snead, Journal of Nuclear Materials 382 (2008), 160-169.

Appendix A

Detailed Quantitative Analysis of the SiC layer

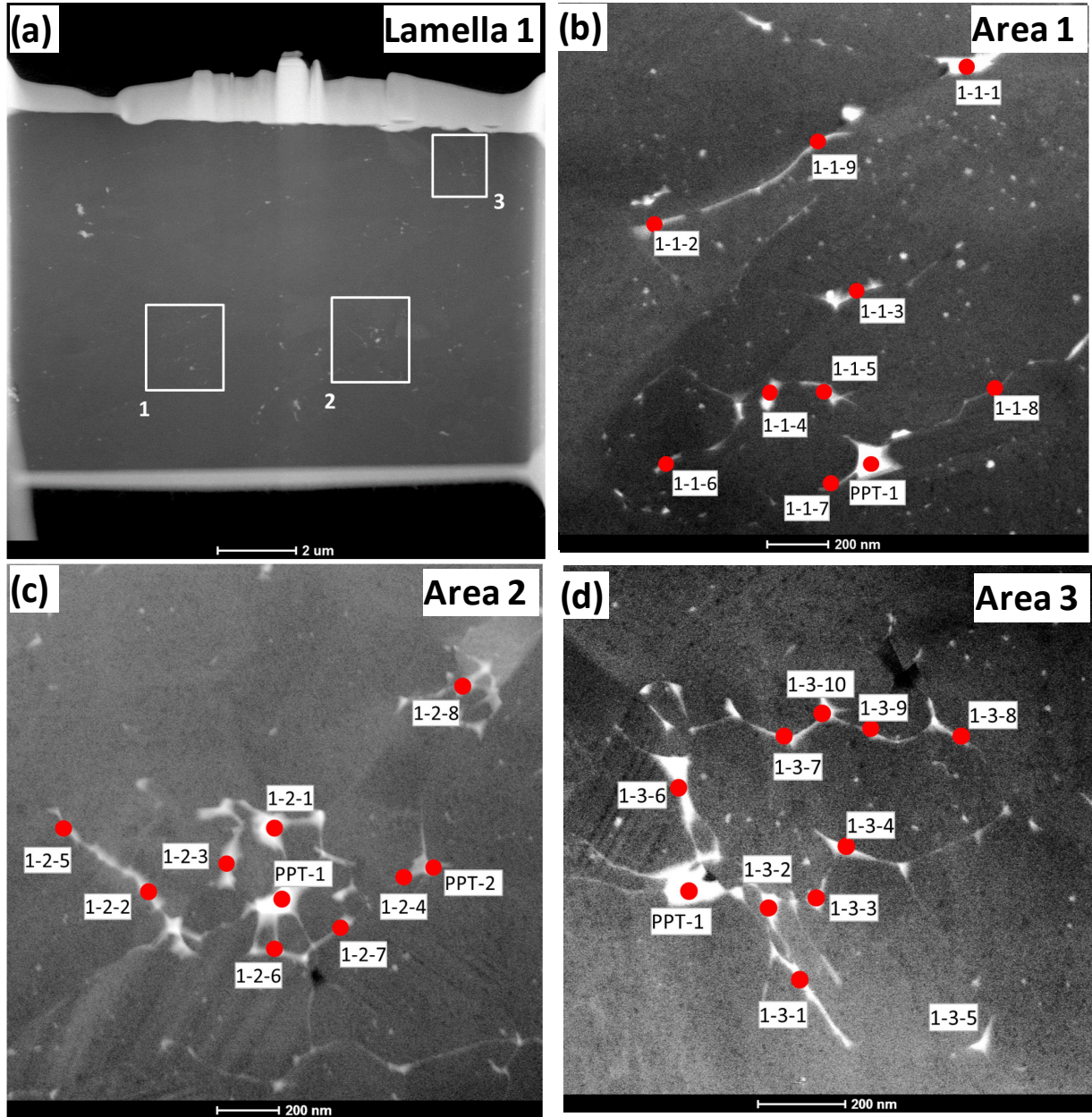


Figure A1. (a) Large field of view STEM dark field image taken from the Lamella 1 fabricated from the SiC/IPyC interface of Location A on TRISO Particle AGR2-222-019. This image shows the areas of interests for the STEM-EDS study. STEM images on (b–d) show the detailed spots for EDS analysis on Area 1, 2, and 3, respectively.

Table A1. Qualitative EDS compositions from the SiC/IPyC interface of Location A from AGR2-222-019, taken from Areas 1, 2, and 3 that are highlighted in Figure A1.

Lamella-1, Area-1													
	Si	C	Zr	Mo	Pd	Ag	Cd	Te	I	Cs	Ce	U	Pu
1-1-1	62.92	32.51	0	0	3.81	0	0	0	0	0		0.47	0.26
1-1-2	67.19	31.1	0	0.05	1.17	0	0.04	0	0	0	0	0.15	0.13
1-1-3	66.93	31.12	0	0	1.23	0.29	0.1	0	0	0	0	0.1	0.18
1-1-4	62.73	34.5	0	0	2.45	0	0	0	0	0	0	0.18	0.11
1-1-5	64.76	32.14	0.03	0	2.85	0.07	0	0	0	0	0	0	0.12
1-1-6	64.85	32.67	0	0.03	2.08	0	0.14	0	0	0.02	0	0	0.18
1-1-7	64.26	33.63	0.23	0	1.71	0.03	0	0	0.03	0	0	0	0.06
1-1-8	67.8	31.58	0.06	0.04	0.28	0.21	0	0	0	0	0	0	0
1-1-9	69.99	27.57	0	0	2.3	0	0	0.03	0.01	0	0	0	0.06
PPT-1	58.7	37.55	0	0	3.26	0	0	0	0	0	0	0.31	0.14
Area-2													
	Si	C	Zr	Mo	Pd	Ag	Cd	Te	I	Cs	Ce	U	Pu
1-2-1	56.73	36.65	5.36	0.55	0.06	0	0	0	0	0	0	0.61	0
1-2-2	64.77	31.52	0.21	0	2.78	0.31	0	0.02	0.01	0	0	0.23	0.09
1-2-3	61.36	32.43	0	0	6.13	0.05	0	0	0	0	0	0	0
1-2-4	62.15	26.19	0	0	11.55	0.09	0	0	0	0	0	0	0
1-2-5	65.87	31.53	0.14	0	2.41	0	0	0	0	0	0	0	0.02
1-2-6	58.4	29.47	0	0	12.02	0.08	0	0	0.01	0	0	0	0
1-2-7	60.13	34.76	0	0	5.05	0.03	0	0	0	0	0	0	0
1-2-8	63.59	31.86	0.1	0	3.67	0.02	0.03	0.08	0	0	0	0.27	0.32
PPT-1	45.38	27.36	0.02	0	27.1	0.12	0	0	0	0	0	0	0
PPT-2	61.92	21.9	0.04	0.04	15.96	0.11	0	0	0	0	0	0	0
Area-3													
	Si	C	Zr	Mo	Pd	Ag	Cd	Te	I	Cs	Ce	U	Pu
1-3-1	64.43	32.83	0.09	0	2.03	0.16	0	0	0	0	0	0.17	0.24
1-3-2	62.83	34.82	0.03	0	1.67	0.16	0	0	0	0	0	0.15	0.31
1-3-3	61.44	33.66	0.02	0	3.63	0.12	0.07	0.07	0	0.02	0	0.48	0.43
1-3-4	63.44	34.2	0.12	0	1.9	0	0.14	0.01	0	0.01	0	0.11	0.03
1-3-5	64.2	33.29	0.08	0	2.27	0.05	0	0.01	0.03	0	0	0	0.02
1-3-6	67.07	29.25	0.01	0	3.65	0	0	0	0	0	0	0	0
1-3-7	64.74	32.92	0.05	0	2.13	0	0	0.02	0	0.08	0	0	0.02
1-3-8	61.53	35.64	0	0	0.7	1.76	0.2	0.05	0	0	0	0	0.08
1-3-9	62.51	34.4	0.07	0	0.36	1.94	0.59	0.08	0.02	0	0	0	0
1-3-10	63.03	30.56	0.03	0	6.26	0	0	0	0	0.04	0	0	0.04

PPT-1	58.98	34.05	0	0	6.03	0	0	0	0	0	0	0.64	0.28
-------	-------	-------	---	---	------	---	---	---	---	---	---	------	------

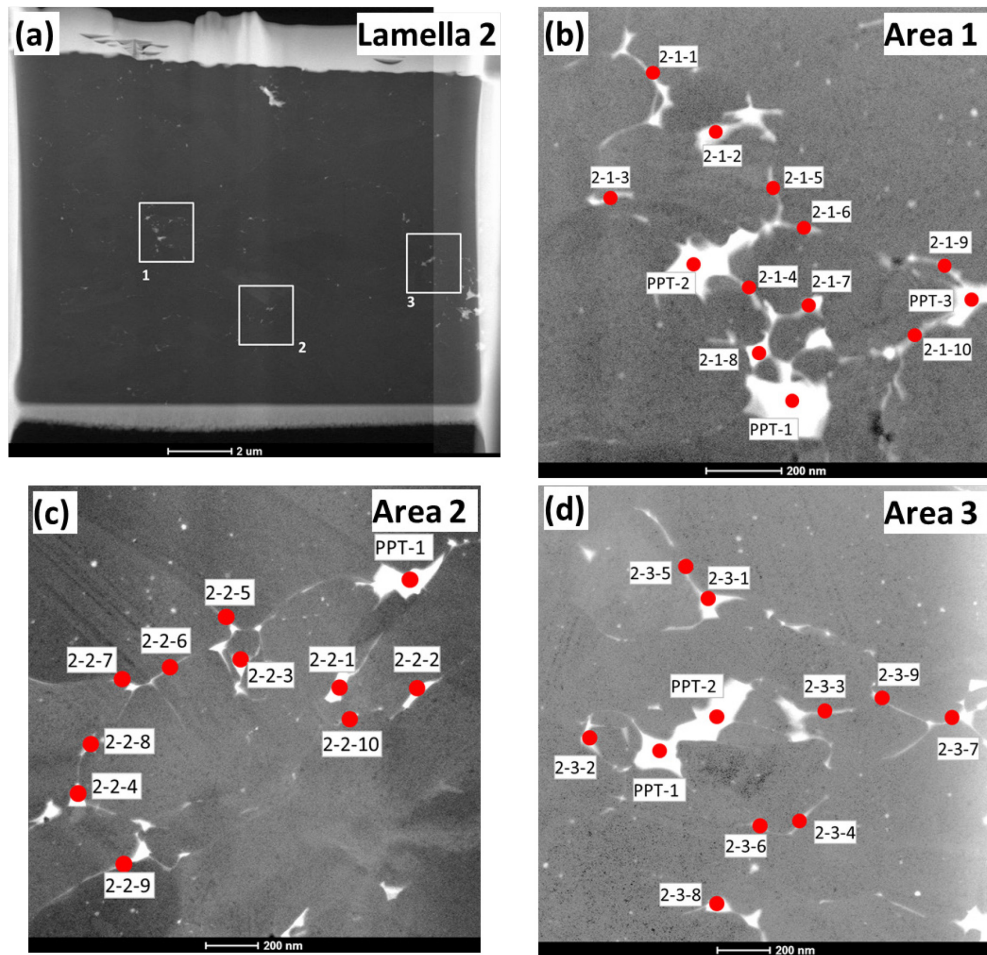


Figure A2. (a) Large field of view STEM dark field image taken from the Lamella 2 fabricated from the center SiC of Location A on TRISO Particle AGR2-222-019. This image shows the areas of interests for the STEM-EDS study. STEM images on (b–d) show the detailed spots for EDS analysis on Area 1, 2, and 3, respectively.

Table A2. Qualitative EDS compositions from the center SiC layer of Location A from AGR2-222-019, taken from Areas 1, 2, and 3 that are highlighted in Figure A2.

Lamella-2, Area-1													
	Si	C	Zr	Mo	Pd	Ag	Cd	Te	I	Cs	Ce	U	Pu
2-1-1	59.1	37.88	0	0	3	0	0	0	0	0	0	0	0
2-1-2	57.16	35.65	0.01	0	7.06	0.1	0	0	0	0	0	0	0
2-1-3	59.29	36.46	0	0	4.09	0	0.09	0	0.05	0	0	0	0
2-1-4	59.13	37.91	0.18	0.05	2.58	0	0	0.01	0.02	0.02	0	0	0.06
2-1-5	58.03	38.34	0.09	0.01	3.5	0	0	0	0	0	0	0	0
2-1-6	62.59	33.84	0	0	3.42	0.05	0	0	0.03	0.03	0	0	0
2-1-7	57.68	33.87	0	0	8.08	0.31	0	0	0	0	0	0.03	0
2-1-8	59.75	32.59	0.01	0.04	7.26	0.1	0.12	0.09	0	0	0	0	0

2-1-9	60.66	36.49	0.03	0.06	2.67	0	0	0	0	0	0	0	0.06
2-1-10	59.75	39.17	0	0.77	0.15	0	0	0.08	0.01	0	0	0.03	0
PPT-1	46.43	38.31	0	0	15.07	0.15	0	0	0	0	0	0	0
PPT-2	43.55	25.09	0	0	31.23	0.08	0	0.03	0	0	0	0	0
PPT-3	49.66	32.87	0	0.01	17.28	0.14	0	0	0	0	0	0	0
Area-2													
	Si	C	Zr	Mo	Pd	Ag	Cd	Te	I	Cs	Ce	U	Pu
2-2-1	79.21	6.99	0	0	13.65	0.13	0	0	0	0	0	0	0
2-2-2	66.16	31.44	0.2	0.11	1.58	0.05	0.07	0.03	0.07	0	0	0.16	0.08
2-2-3	66.05	29.78	0.16	0	3.52	0	0.05	0	0	0	0	0.12	0.28
2-2-4	61.65	30.97	0	0	5.77	0	0	0.04	0.09	0	0	0.82	0.62
2-2-5	76.64	30.1	0.03	0	1.53	0.14	0.01	0	0	0	0	0.07	0.08
2-2-6	82.08	32.44	0	0	0.21	0	0	0	0	0	0	0	0
2-2-7	65.26	30.55	0	0	3.86	0	0	0	0	0	0	0.12	0.19
2-2-8	69.13	25.87	0.02	0	4.75	0.03	0	0.01	0	0	0	0.16	0
2-2-9	60.71	23.72	0.07	0.01	15.25	0.08	0	0	0	0.05	0	0	0.07
2-2-10	65.06	27.9	0.07	0.01	6.7	0.05	0	0	0	0	0	0.11	0.06
PPT-1	69.38	19.01	0	0	11.49	0.09	0	0	0	0	0	0	0.01
Area-3													
	Si	C	Zr	Mo	Pd	Ag	Cd	Te	I	Cs	Ce	U	Pu
2-3-1	64.78	30.45	0.02	0	4.66	0	0	0	0	0	0	0	0.04
2-3-2	64.62	31.69	0.01	0	3.27	0	0	0	0	0	0	0.17	0.21
2-3-3	66.16	31.65	0.02	0	2.11	0	0.01	0	0	0	0	0	0.01
2-3-4	67.6	30.53	0.13	0	1.62	0	0	0	0.02	0	0	0	0.06
2-3-5	68.18	29.53	0	0	1.93	0	0.24	0	0	0.07	0	0	0.01
2-3-6	64.42	29.97	0	0	4.01	0	0.26	0	0	0	0	0.57	0.74
2-3-7	69.32	24.92	0.05	0	5.59	0.04	0	0	0	0	0	0.01	0.02
2-3-8	62.12	30.19	0.09	0	6.02	0	0	0.16	0	0	0	0.59	0.8
2-3-9	69.16	25.99	0.12	0	4.57	0	0.09	0	0	0.02	0	0	0.02
PPT-1	57.37	36.48	0	0	4.71	0	0	0	0	0	0	0.85	0.54
PPT-2	62.99	24.62	0	0.03	10.07	0	0	0.05	0.01	0	0	1.42	0.77

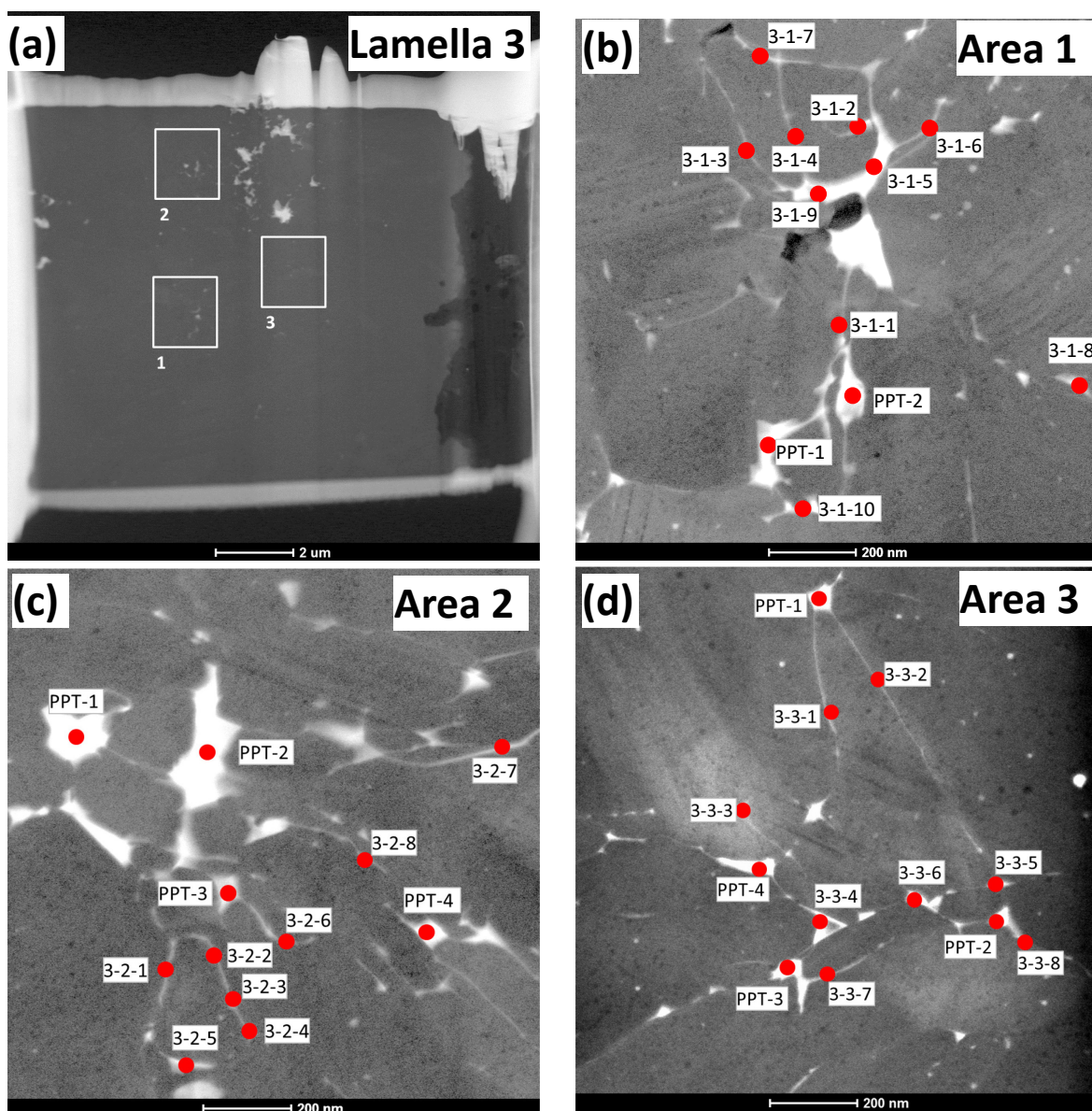


Figure A3. (a) Large field of view STEM dark field image taken from the Lamella 3 fabricated from the outer SiC/OPyC interface of Location A of the TRISO Particle AGR2-222-019. This image shows the areas of interests for STEM-EDS study. STEM images on (b-d) shows the detailed spots for EDS analysis on Area 1, 2, and 3, respectively.

Table A3. Qualitative EDS compositions from the outer SiC/OPyC layer of Location A from AGR2-222-019, taken from Areas 1,2 and 3 that are highlighted in Figure A3.

Lamella-3, Area-1													
	Si	C	Zr	Mo	Pd	Ag	Cd	Te	I	Cs	Ce	U	Pu
3-1-1	64.08	25.15	0.01	0	10.59	0.12	0	0	0	0	0	0	0
3-1-2	68.39	29.49	0	0	1.87	0.04	0	0	0	0	0	0.09	0.08
3-1-3	69.6	29.54	0	0	0.83	0	0	0	0	0	0	0	0
3-1-4	64.41	34.62	0.01	0	0.93	0	0	0	0	0	0	0	0

3-1-5	66.42	30.5	0	0	3.03	0.03	0	0	0	0	0	0	0
3-1-6	68.74	30.17	0	0	1.04	0	0	0	0.01	0	0	0	0.02
3-1-7	67.02	29.17	0.01	0	3.77	0	0	0	0	0	0	0	0
3-1-8	64.06	31.78	0	0	4.12	0.02	0	0	0	0	0	0	0
3-1-9	61.02	25.82	0	0.01	13.06	0.02	0.02	0.01	0	0	0	0	0
3-1-10	62.34	27.55	0.04	0.01	9.99	0.03	0	0	0	0	0	0	0
PPT-1	63.55	25.74	0	0	10.49	0.18	0	0	0	0.02	0	0	0
PPT-2	57.79	57.79	10.54	0	0.32	0	0	0.04	0.06	0	0	0.79	0
Area-2													
	C	Si	Zr	Mo	Pd	Ag	Cd	Te	I	Cs	Ce	U	Pu
3-2-1	37.81	61.52	0	0	0.65	0	0	0	0	0	0	0	0
3-2-2	30.57	67.13	0	0.02	0.47	1.28	0.44	0	0	0	0	0	0.05
3-2-3	32.93	66.14	0.01	0	0.9	0	0	0	0	0	0	0	0
3-2-4	27.98	69.17	0	0	2.62	0.03	0.06	0	0	0.04	0	0	0.07
3-2-5	28.16	67.52	0.03	0	4.15	0	0	0	0.02	0.06	0	0	0.03
3-2-6	27.31	69.23	0.05	0	2.59	0.34	0.24	0	0	0.06	0	0.01	0.12
3-2-7	30.2	67.42	0.03	0	2.29	0	0.01	0	0	0	0	0	0.01
3-2-8	34.89	64.92	0	0	0.17	0	0	0	0	0	0	0	0
PPT-1	16.91	52.39	0.45	0	28.46	1.25	0.11	0	0.05	0	0	0	0.35
PPT-2	23.42	67.67	0.2	0	8.19	0.16	0	0	0	0	0	0	0.33
PPT-3	32.27	65.34	0	0	2.34	0	0.01	0	0	0	0	0	0.01
PPT-4	28.2	65.7	0	0	5.32	0	0	0.01	0	0	0	0.44	0.3
Area-3													
	C	Si	Zr	Mo	Pd	Ag	Cd	Te	I	Cs	Ce	U	Pu
3-3-1	25.73	73.73	0	0	0.52	0	0	0	0	0	0	0	0
3-3-2	26.64	72.92	0.02	0	0.24	0.07	0	0	0	0.01	0	0.05	0
3-3-3	25.83	71.64	0.03	0.01	2.34	0.02	0.02	0	0	0	0	0.04	0.01
3-3-4	27.98	71.02	0	0	0.97	0	0	0	0	0	0	0	0
3-3-5	25.69	72.45	0	0	1.64	0	0	0	0	0	0	0.07	0.12
3-3-6	25.33	70.34	0	0	3.12	0	0	0	0	0.02	0	0.71	0.46
3-3-7	24.74	74.76	0.02	0	0.37	0	0	0.02	0	0	0	0.02	0.03
3-3-8	27.18	71.35	0	0.02	1.33	0.1	0	0	0	0	0	0	0
PPT-1	26.26	73.02	0.04	0.01	0.49	0	0.06	0	0	0	0	0.08	0
PPT-2	26.69	70.24	0	0	2.87	0.01	0	0	0	0	0	0.06	0.1

PPT-3	19.37	70.67	0.12	0	7.67	0	0	0.08	0	0	0	0.74	1.32
PPT-4	23.78	69.55	0	0	5.08	0	0	0.11	0.01	0	0	1	0.43

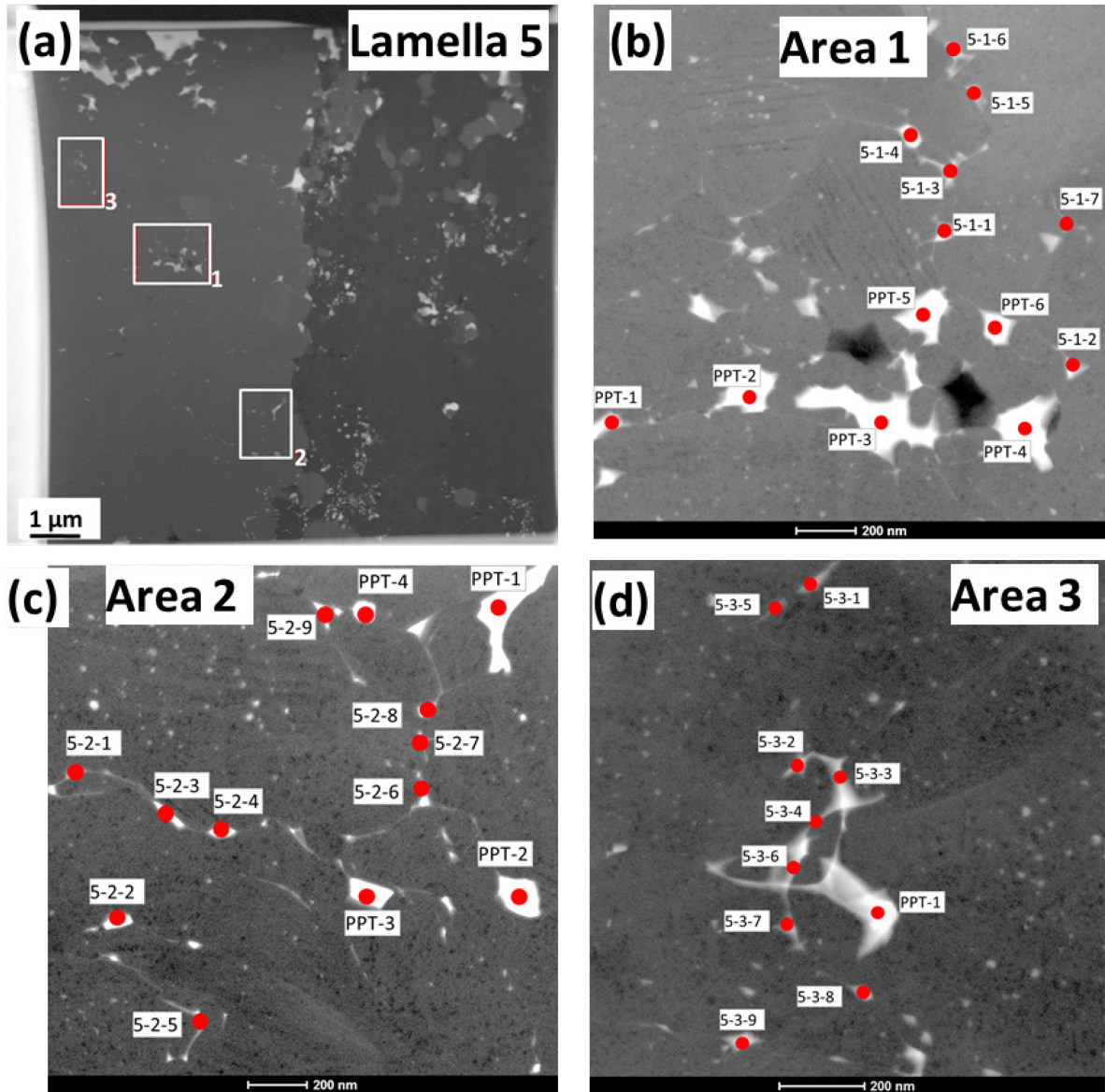


Figure A4. (a) Large field of view STEM dark field image taken from the Lamella 5 fabricated from the SiC/IPyC interface of Location A on TRISO Particle AGR2-222-019. This image shows the areas of interests for STEM-EDS study. STEM images on (b–d) shows the detailed spots for EDS analysis on Area 1, 2, and 3, respectively.

Table A4. Qualitative EDS compositions from the SiC/IPyC interface of Location B from AGR2-222-019, taken from Areas 1, 2, and 3 that are highlighted in Figure A4.

Lamella-5, Area-1													
	C	Si	Zr	Mo	Pd	Ag	Cd	Te	I	Cs	Ce	U	Pu

5-1-1	33.83	61.52	0	0	3.34	0	0	0	0	0	0	0.96	0.32
5-1-2	28.16	63.52	0	0	7.4	0	0.13	0	0.05	0	0	0.03	0.68
5-1-3	28.1	63.65	0	0	7.9	0.03	0.01	0	0	0	0	0	0.3
5-1-4	4.81	84.15	1.7	0.63	0	0	0	0	0	0.03	0	8.62	0.01
5-1-5	30.6	67.42	0	0	1.45	0	0.06	0	0	0.03	0	0.26	0.15
5-1-6	29.75	63.69	0	0	6.12	0	0	0	0	0	0	0.25	0.17
5-1-7	27.9	64.56	0	0.02	6.89	0.02	0.48	0.01	0	0	0	0	0.07
PPT-1	34.06	56.68	0	0	7.04	0	0	0	0	0	0	1.76	0.43
PPT-2	39.08	46.41	0.03	0	9.91	0	0	0	0	0	0	3.64	0.91
PPT-3	29.04	48.72	0	0	13.2	0	0	0.04	0	0	0	6.52	2.46
PPT-4	32.26	53.67	0	0	8.99	0	0	0	0	0	0	4.03	1.02
PPT-5	32.85	58.45	0	0	6.17	0	0	0	0	0	0	2.12	0.39
PPT-6	13.63	64.59	0	0	12.7	0.37	0	0.19	0	0.23	0	6.09	2.15
Area-2													
	Si	C	Zr	Mo	Pd	Ag	Cd	Te	I	Cs	Ce	U	Pu
5-2-1	44.53	51.27	0	0	2.79	0	0	0	0	0	0	1.26	0.13
5-2-2	40.01	53.13	0	0	5.03	0	0	0	0	0	0	1.42	0.39
5-2-3	38.74	56.58	0	0	3.45	0.01	0	0	0	0	0	1.01	0.17
5-2-4	33.91	55.18	0	0	6.47	0.12	0	0.08	0	0.02	0	2.9	1.26
5-2-5	39.52	54.75	0.02	0	5.57	0	0	0	0	0	0	0	0.11
5-2-6	37.69	59.95	0	0	1.77	0	0	0	0	0	0	0.29	0.27
5-2-7	33.02	57.61	0.08	0	6.13	0.18	0.08	0.21	0	0.01	0	1.58	1.06
5-2-8	38.64	59.64	0.01	0	1.41	0	0	0	0	0	0	0.25	0.02
5-2-9	37.19	59.75	0	0	2.9	0.02	0	0	0	0	0	0	0.11
PPT-1	33.83	52.62	0	0	9.57	0	0	0	0	0	0	3.44	0.52
PPT-2	37.79	55.12	0	0	5.05	0	0	0	0	0	0	1.77	0.24
PPT-3	41.29	49.98	0	0	6.11	0	0	0	0	0.01	0	2.01	0.56
PPT-4	26.16	58.51	0	0	9.22	0	0	0.24	0	0.13	0	4.2	1.5
Area-3													
	C	Si	Zr	Mo	Pd	Ag	Cd	Te	I	Cs	Ce	U	Pu
5-3-1	32.25	64.43	0	0	2.16	0	0.02	0.05	0	0	0	0.66	0.4
5-3-2	26.35	69.18	0	0	4.26	0	0	0	0	0	0	0	0.19
5-3-3	29.74	66.52	0	0	3.38	0	0	0	0.03	0	0	0.09	0.19
5-3-4	29.95	66.55	0	0	2.32	0	0.16	0.12	0	0	0	0.5	0.37
5-3-5	29.54	68.93	0	0	1.4	0	0	0	0	0	0	0.05	0.05
5-3-6	69.63	29.4	0	0	0.85	0	0	0	0	0	0	0.06	0.05
5-3-7	30.72	67.77	0	0	1.11	0	0	0	0	0	0	0.2	0.17
5-3-8	36.38	60.38	0	0	2.23	0	0	0	0	0	0	0.82	0.17

5-3-9	28.34	64.6	0	0	4.55	0.45	0.12	0	0.01	0	0	1.52	0.38
PPT-1	24.37	59	0	0.5	12.58	0	0	0.08	0	0	0	2.38	1.06

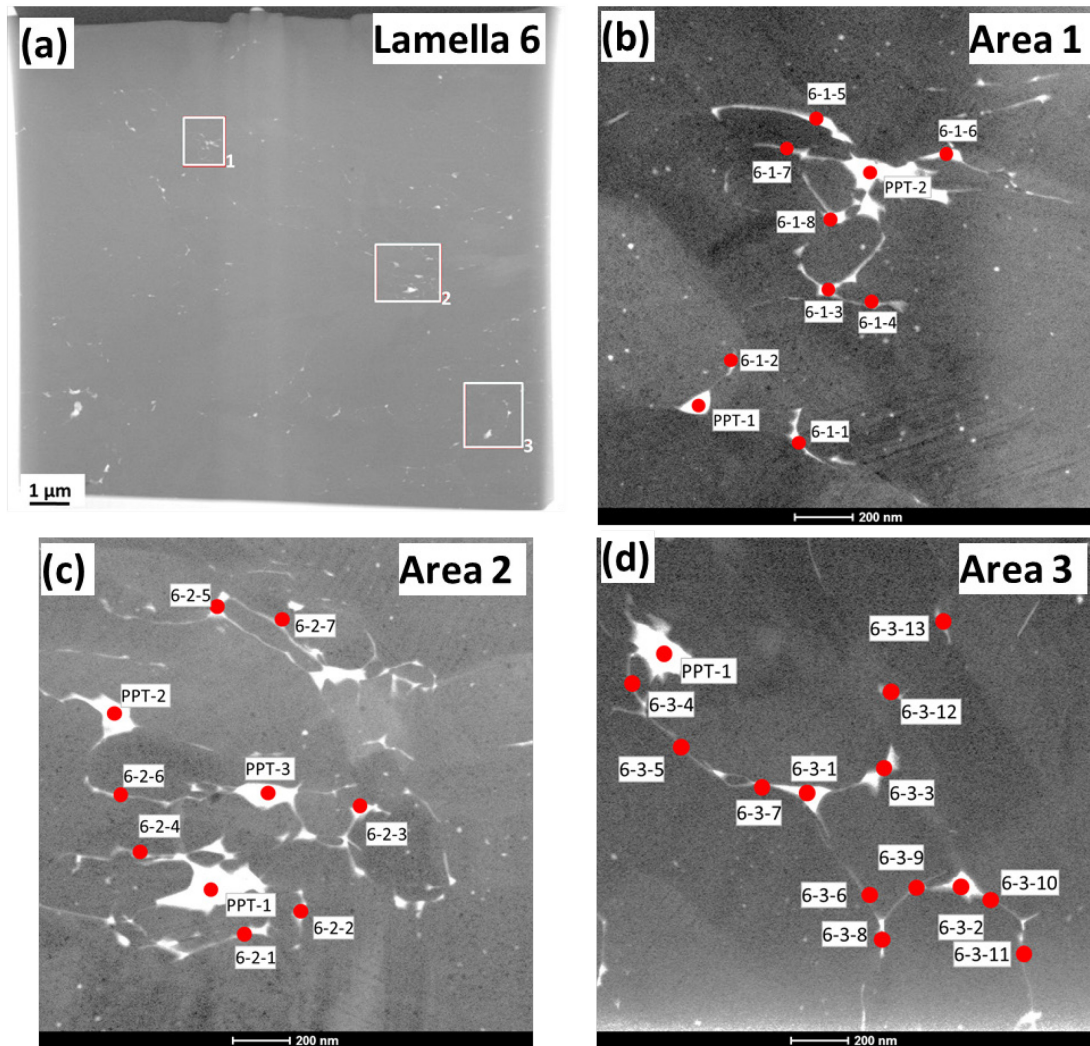


Figure A5. (a) Large field of view STEM dark field image taken from the Lamella 6 fabricated from the center SiC of Location B of the TRISO Particle AGR2-222-019. This image shows the areas of interests for STEM-EDS study. STEM images on (b-d) shows the detailed spots for EDS analysis on Area 1, 2, and 3, respectively.

Table A5. Qualitative EDS compositions from the center SiC layer of Location B from AGR2-222-019, taken from Areas 1,2 and 3 that are highlighted in Figure A5.

Lamella-6, Area-1													
	C	Si	Zr	Mo	Pd	Ag	Cd	Te	I	Cs	Ce	U	Pu
6-1-1	32.86	63.43	0	0	3.68	0	0	0	0	0	0	0	0.01
6-1-2	31.91	67.43	0	0	0.33	0.06	0	0	0	0	0	0.02	0.22
6-1-3	37.95	61.49	0	0	0.55	0	0	0	0	0	0	0	0
6-1-4	30.51	67.06	0.06	0	2.02	0	0.03	0	0	0	0	0.06	0.21

6-1-5	33.42	59.46	0	0	6.26	0.01	0	0.01	0	0	0	0.38	0.43
6-1-6	34.2	60.22	0.14	0	3.94	0.22	0	0.16	0.07	0	0	0.38	0.61
6-1-7	32.39	65.13	0.04	0	1.93	0	0.04	0.04	0	0	0	0	0.39
6-1-8	33.31	59.75	0.12	0	6.57	0.15	0	0	0	0	0	0	0.07
PPT-1	12.06	75.37	0	0	9.73	0.03	0	0.12	0.07	0	0	1.59	0.99
PPT-2	26.75	65.97	0	0	6.41	0	0	0	0	0	0	0.33	0.51
Area-2													
	C	Si	Zr	Mo	Pd	Ag	Cd	Te	I	Cs	Ce	U	Pu
6-2-1	32.95	56.32	0	0.04	10.37	0.18	0.05	0	0	0.03	0	0.03	0
6-2-2	37.65	61.14	0	0	1.05	0	0	0	0	0	0	0.07	0.06
6-2-3	33.31	61.15	0.19	0	4.03	0	0.22	0.08	0	0	0	0.23	0.75
6-2-4	31.92	66.75	0.03	0.79	0.41	0.08	0	0	0	0	0	0	0
6-2-5	33.65	63.82	0.04	0	2.24	0.01	0.01	0	0	0	0	0.04	0.16
6-2-6	36.11	61.62	0	0	2.08	0	0	0	0	0	0	0.04	0.13
6-2-7	35.77	63.04	0	0	1.09	0	0	0	0	0	0	0.01	0.06
PPT-1	44.04	44.23	0	0	8.37	0	0	0	0	0.03	0	2.46	0.84
PPT-2	31.23	57.47	0	0	11.24	0.03	0	0	0	0	0	0	0
PPT-3	23.53	64.26	0	0	9.77	0	0	0.04	0	0	0	1.19	0
Area-3													
	C	Si	Zr	Mo	Pd	Ag	Cd	Te	I	Cs	Ce	U	Pu
6-3-1	25.2	53.65	0.15	0.01	20.19	0.48	0	0	0	0.05	0	0	0.23
6-3-2	32.85	58.45	0	0	8.61	0.06	0	0	0	0	0	0	0
6-3-3	20.96	67.78	0.18	0	9.41	1.41	0	0	0	0	0	0	0.23
6-3-4	42.61	56.13	0.01	0	1.18	0.02	0	0	0	0	0	0	0.01
6-3-5	38.71	61.27	0	0	0	0	0	0	0	0	0	0	0
6-3-6	33.64	65.75	0	0	0.55	0	0	0.04	0	0	0	0	0
6-3-7	35.59	58.64	0.28	0	4.63	0.07	0	0	0	0	0	0.26	0.49
6-3-8	32.2	65.78	0.11	0	1.43	0.25	0.13	0	0.06	0	0	0.01	0
6-3-9	35.43	55.11	0	0.01	9.34	0.09	0	0	0	0	0	0	0
6-3-10	43.06	56.85	0	0	0.08	0	0	0	0	0	0	0	0
6-3-11	44.19	54.66	0	0	1.14	0	0	0	0	0	0	0	0
6-3-12	40.42	58.89	0.03	0	0.65	0	0	0	0	0	0	0	0
6-3-13	34.41	63.9	0.02	0	1.04	0	0.23	0	0	0	0	0.17	0.19
PPT-1	43.83	48.39	0.11	0	5.41	0	0	0	0	0.02	0	1.29	0.92

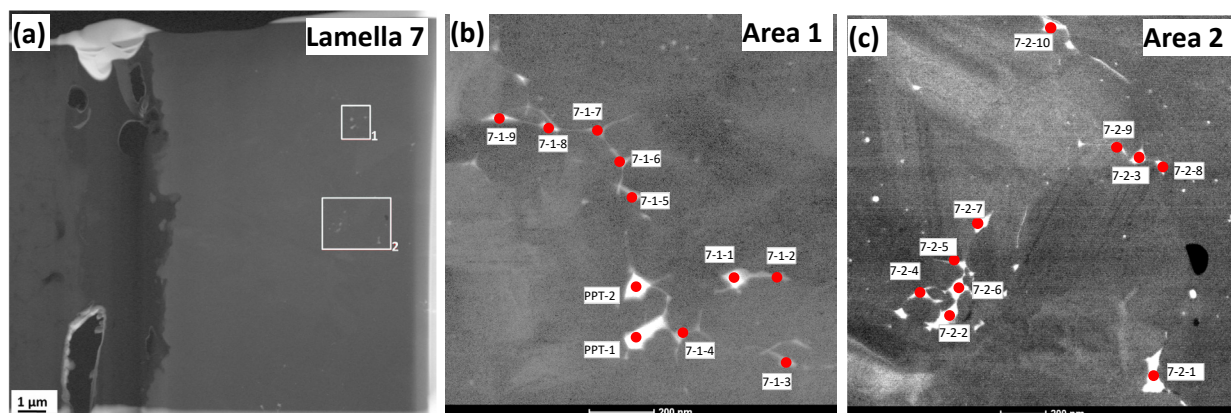


Figure A6. (a) Large field of view STEM dark field image taken from the Lamella 7 fabricated from the outer SiC/OPyC interface of Location A on TRISO Particle AGR2-222-019. This image shows the areas of interests for the STEM-EDS study. STEM images (b–d) show the detailed spots for EDS analysis on Area 1, 2, and 3, respectively.

Table A6. Qualitative EDS compositions from the outer SiC/OPyC layer of Location B from AGR2-222-019, taken from Areas 1 and 2 that are highlighted in Figure A6.

Lamella-7, Area-1													
	C	Si	Zr	Mo	Pd	Ag	Cd	Te	I	Cs	Ce	U	Pu
7-1-1	39.3	54.78	0	0	4.29	0.26	0	0.15	0.12	0	0	0.44	0.62
7-1-2	38.18	59.86	0	0	1.94	0	0	0	0	0	0	0	0
7-1-3	41.21	55.68	0.27	0	2.48	0	0	0	0.08	0	0	0.11	0.13
7-1-4	34.23	61.53	0	0.02	3.51	0	0	0	0	0	0	0	0.68
7-1-5	43.86	54.06	0	0	1.89	0	0	0	0	0	0	0.03	0.14
7-1-6	36.28	60.2	0.12	0.2	2.71	0.38	0	0	0.04	0.02	0	0	0.01
7-1-7	39.09	58.92	0	0	1.98	0	0	0	0	0	0	0	0
7-1-8	38.73	58.24	0	0	2.73	0	0	0	0	0	0	0.13	0.14
7-1-9	39.65	56.58	0	0	3.39	0	0	0	0	0	0	0.15	0.2
PPT-1	39.38	51.57	0	0	8.97	0.06	0	0	0	0	0	0	0
PPT-2	29.03	58.88	0	0	9.51	0	0.17	0.18	0	0	0	1.15	1.04
Area-2													
	C	Si	Zr	Mo	Pd	Ag	Cd	Te	I	Cs	Ce	U	Pu
7-2-1	37.61	56.09	0	0	4.58	0.83	0	0	0	0	0	0.36	0.51
7-2-2	42.39	51.7	0	0	4.58	0.23	0.06	0	0	0	0	0.68	0.32
7-2-3	41.98	53.25	0	0	3.84	0	0	0.08	0.06	0	0	0.47	0.27
7-2-4	47.54	49.8	0	0	2.09	0	0.15	0	0	0	0	0.16	0.23
7-2-5	42.96	55.17	0	0.07	1.57	0	0	0	0	0	0	0.04	0.15
7-2-6	40.43	50.26	0	0	9.2	0.09	0	0	0	0	0	0	0
7-2-7	41.93	52.93	0.03	0	3.99	0.03	0	0.06	0	0	0	0.53	0.46
7-2-8	46.22	52.44	0	0	1.11	0	0	0	0	0	0	0	0.21

7-2-9	45.04	50.05	0	0.01	3.7	0.2	0	0	0	0.14	0	0.56	0.25
7-2-10	44.24	51.91	0	0	3.37	0	0	0	0	0	0	0.26	0.2